UNIVERSITY OF COLOGNE

Master Thesis

Tradeoff-Induced Fitness Landscapes with Diminishing Returns Epistasis

Muna Turki

Supervisor and First Examiner:
Prof. Dr. Joachim Krug
Second Examiner:
Prof. Dr. Tobias Bollenbach

University of Cologne
Institute for Biological Physics
October 16, 2024

Abstract

The Tradeoff-Induced Landscapes (TIL) model uses tradeoff between the costs and benefits of mutations to describe an environment-dependent fitness landscape through a parameterized function. This model has been successful in generating highly rugged and highly accessible landscapes, which are key features observed in a growing body of experimental results. Recent experimental data was analyzed in this context, and found to strongly encode diminishing returns epistasis in the parameters of the fitness function, namely the mutation cost and resistance proxies. While fitness itself showed a dominant positive epistasis trend. In an attempt to model the results, the TIL model framework was used to introduce diminishing returns epistasis into the parameters of fitness which allowed the emergence of a positive epistasis trend in fitness, this new model will be called the TILME model. The evolutionary dynamics and the landscape properties of the TILME model have been studied in two simplified cases. The violations of accessibility as defined by the TIL model were identified. This study also provides insight into the landscape ruggedness, where it was found that the number of potential peaks in a landscape decreases with increasing levels of epistatic interactions.

Acknowledgement

I am deeply grateful to the BCGS program for providing me with this life-changing opportunity to pursue my degree without financial worries. My sincere thanks go to Joachim Krug for his invaluable guidance, advice, and unwavering support throughout my journey. I am also thankful to Suman Das, Muhitten Mungan, and Rotem Gross for their dedication in answering my questions and engaging in thoughtful discussions. To each member of the group, thank you for making the daily office routine something I genuinely looked forward to. To the wonderful friends I found in Cologne—Sreya, Ram, Katharina, Luis, and Nils—thank you for filling this experience with joy and unforgettable moments. A special thank you to Sreya, Ram, Katharina, Nils, Daniel and Rotem for their help in proofreading this work. Finally, to Husn, dad, mom, May, Amira and Ahmed, my awesome family whose love and support have been my foundation throughout—I love you!

Contents

List of Figures

List of Tables

Abbreviation List

Abbreviation	Full Term
AMR	Antimicrobial Resistance
GDP	Gross Domestic Product
IP	Intersection Point
MIC	Minimum Inhibitory Concentration
IC_{50}	Half-Maximal Inhibitory Concentration
TIL	Tradeoff-Induced Landscapes
TILME	Tradeoff-Induced Landscapes with Magnitude Epistasis

1 Introduction

The discovery of Penicillin in the early 20th century brought tremendous success to humanity's battle against pathogens, enabling the treatment of bacterial infections. Growing evidence since the 1960s suggests that the antibiotics breakthrough is being increasingly compromised by the development of Antimicrobial Resistance (AMR), posing a threat to humans, livestock, and crops. The risk to public health and global development is alarming, with experts fearing that, by 2050, AMR will directly cause up to 10 millions deaths per year [1], eight times the current annual rate of 1.27 million per year [2]. Furthermore, AMR poses a risk to the global economy with a potential loss of around 4% of the global annual Gross Domestic Product (GDP) by 2050, pushing 27 million more people to the verge of extreme poverty [3].

One important mechanism for bacteria to acquire AMR is through the accumulation of point-mutations. A resistant strain of Staphylococcus aureus is an example, where S. aureus is a leading cause of skin and soft tissue infections typically treated by Vancomycin antibiotics. This strain was found to have developed 35 point-mutations distinguishing it from its sensitive counterpart, and these mutations evolved in just three months within an infected patient [4].

In recent decades, a growing effort has been made to understand AMR through developing theoretical models. One class of models that have gained increasing attention are the fitness landscapes, first introduced by Sewall Wright in the 1930s [5]. Fitness landscapes describe evolution as a search process on a high-dimensional sequence space representing mutation scenarios. These models are now widely applied in optimization problems. In evolutionary biology, fitness landscapes provide a framework for predictability of evolution through determinant features such as the abundance of fit genotypes and how accessible they are from other genotypes [6, 7].

Fitness functions defining the search process on the landscape are of central importance. They guide evolution and control the structure of the landscapes. In order to understand environment-driven evolution, we work with a fitness function that depends on the environment. In the context of AMR, our variable is the concentration of antibiotics in which the bacterial population grows.

The endangering pressure of antibiotics directs bacterial cultures towards

the selection of resistant mutants. These resistant mutants are equipped with mutations that increase the fitness of bacteria in the presence of antibiotics allowing for adaptation. However, they usually come with a cost in the form of reduced fitness in the absence of antibiotics. This is due to the fact that resistant mechanisms developed by the mutant bacteria tend to be costly, creating a tradeoff that the mutant has to endure. The fitness functions of interest in this work are those that are parameterized based on this tradeoff assumption, as described in the Tradeoff-Induced Landscapes (TIL) model [8].

This work is divided into two parts. Chapter 3 is dedicated to the analysis of an evolution experiment guided by the TIL model framework. Theoretical modeling of observed fitness is discussed along with the challenges posed by the experimental setting and the difficulty of extracting a stable measure for fitness. The novelty in the chapters 4 and 5 lies in the introduction of diminishing returns epistasis to the existing TIL model.

Diminishing returns epistasis indicates the reduction in the benefit of an advantageous mutation when it occurs in a relatively fit genotype compared to its effect in a relatively unfit genotype. Diminishing returns epistasis has been found to dominate the experimental parameters of fitness. Furthermore, it is increasingly recognized in the literature as a strong feature of adaptation [9, 10]. TIL landscapes with diminishing returns epistasis of simplified fitness functions were theoretically studied, in an attempt to understand the new landscapes properties compared to the TIL model. The fitness functions studied were simplified by first assuming that all mutations are identical in terms of carrying the same cost and contributing the same to the resistance, and later by allowing the cost of mutations to vary randomly.

2 Fitness Models: TIL Model and Terminology

This chapter presents the notation used in the following chapters. In addition, the key terms are defined and introduced in the context of the TIL model.

2.1 The TIL Model

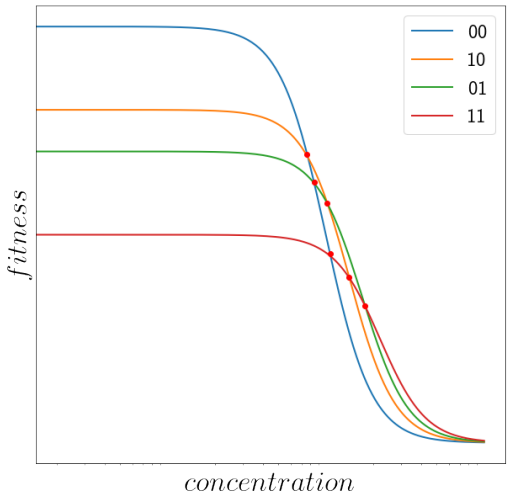

Figure 1: Dose-response curves of four genotypes representing a full system of two possible mutations. The intersection points (IPs) between all pairs of curves are highlighted by light red dots, some of which indicate the change in the role of the fittest.

In a mixed population of different genotypes, the fittest genotypes will dominate the population. Genotypes are defined by a binary sequence $\boldsymbol{\sigma}$, of length L, indicating the presence or the absence of a set of L mutations. These mutations are assumed to enhance the resistance of bacteria against a given antibiotic. The sequence $\boldsymbol{\sigma}$ defines a set of present mutations I^+ and a set of absent mutations I^-. Adopting the notation in [11],

$$I^+(\boldsymbol{\sigma}) = \{i : \sigma_i = 1\} \tag{1}$$

and its complement

$$I^{-}(\boldsymbol{\sigma}) = \{j : \sigma_j = 0\} \tag{2}$$

where $\sigma_i \in \{0, 1\}$, indicating the absence ($\sigma_i = 0$) or the presence ($\sigma_i = 1$) of the mutation i.

Fitness, defined as a genotype's reproductive capacity, is a function of the environment. The fitness of a bacterial population $\boldsymbol{\sigma}$ growing under different concentrations of antibiotics is described by a dose-response curve (Fig. 1). This curve is parameterized by the null-fitness ($r_{\boldsymbol{\sigma}}$) and the IC_{50} or the concentration at which the fitness reduces by half ($m_{\boldsymbol{\sigma}}$). The fitness function is a function of the concentration x and takes the shape of a Hill function [12],

$$f_{\boldsymbol{\sigma}}(x) = \frac{r_{\boldsymbol{\sigma}}}{1 + (\frac{x}{m_{\boldsymbol{\sigma}}})^{\alpha}} \tag{3}$$

where α governs the steepness of the function.

In the Tradeoff-Induced Landscapes (TIL) model [8], each mutation i comes with an advantage in the IC_{50} ($m_i > 1$) and a disadvantage in the null-fitness ($r_i < 1$), a tradeoff between resistance to high concentration and viability in the absence of antibiotic stress. The units are chosen here so that for the wild type $r_i = 1$ and $m_i = 1$. In addition, the model assumes that mutations introduce a non-epistatic effect, meaning that they act independent of each other. Upon accumulation of mutations the total effect is multiplicative,

$$m_{\boldsymbol{\sigma}} = \prod_{i \in I^{+}} m_i \quad and \quad r_{\boldsymbol{\sigma}} = \prod_{i \in I^{+}} r_i. \tag{4}$$

Eq (4) ensures that while $m_{\boldsymbol{\sigma}}$ increases $r_{\boldsymbol{\sigma}}$ decreases.

A key term here is *fitness landscapes*, which are maps from the genotype sequence to its fitness; $f : \boldsymbol{\sigma} \in \mathbb{H}_2^L \rightarrow f(\boldsymbol{\sigma}) \in \mathbb{R}$, where $\mathbb{H}$ is the Hamming space of a binary sequence of L loci. In other words, a fitness landscape induces an acyclic orientation of the sequence space. Fitness landscapes are visualized through a fitness graph where each edge connecting two neighboring sequences, differing by a single mutation, is directed towards increasing fitness (Fig 2).

A bacterial population is assumed to evolve in a strong selection weak mutation regime of evolution [13]. Populations in this regime are assumed to evolve by acquiring one mutation at a time, which subsequently dominates the

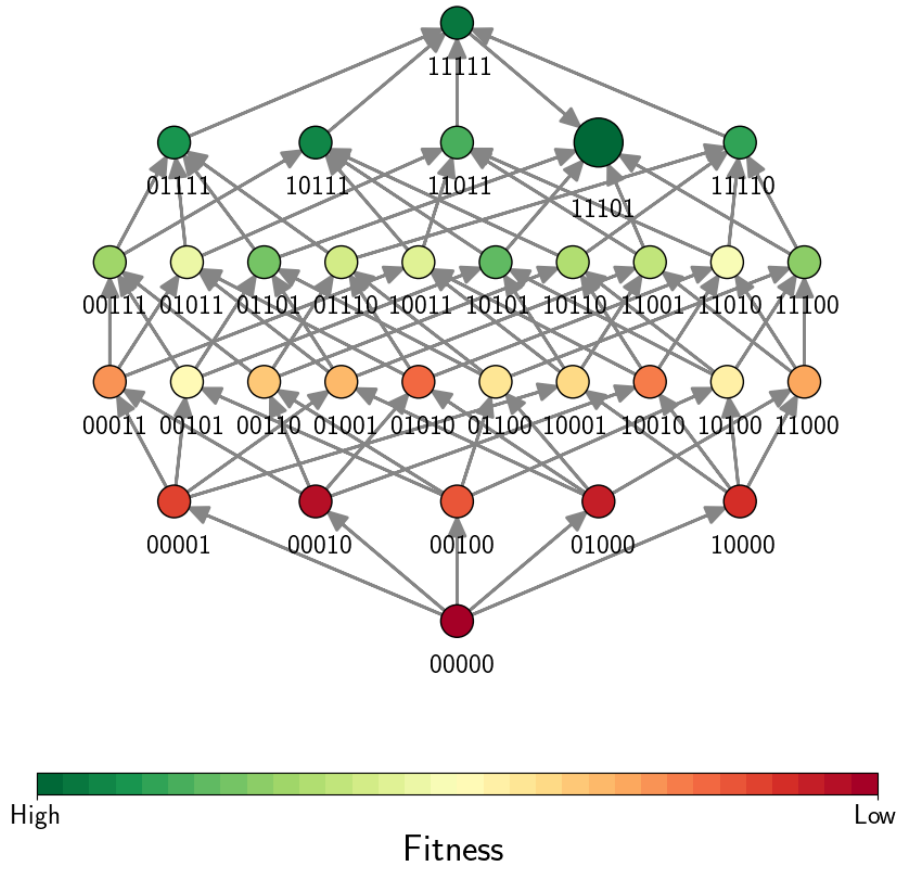

Figure 2: Example of a fitness landscape graph with genotype (11101) as a peak. The color coding refers to the fitness of the genotype.

population. Fitness landscapes portray this selection process, like the example in Figure 2, where a population takes a single step mutation seeking a fitness peak in a static environment.

Peakness here is a property of a genotype. A peak is fitter than all neighbouring genotypes which it could reach by acquiring or removing a mutation. A genotype $\boldsymbol{\sigma}$ is a fitness peak at concentration x if

$$f_{\boldsymbol{\sigma}}(x) > f_{\boldsymbol{\sigma}^{-i}}(x) \text{ and } f_{\boldsymbol{\sigma}}(x) > f_{\boldsymbol{\sigma}^{+j}}(x), \tag{5}$$

where $\boldsymbol{\sigma}^{-i}$ ($\boldsymbol{\sigma}^{+j}$) is a genotype identical to $\boldsymbol{\sigma}$ except lacking a mutation $i \in I^{+}$ (having an additional mutation $j \in I^{-}$). As the environment changes, so does the fitness of each genotype (eq. 3) along with the peakness structure of the fitness landscape.

Important evolutionary dynamics can be inferred from the fitness landscape, such as how frequent fitness peaks are (ruggedness) and how reachable they are from other genotypes (accessibility).

To study how a population evolves on such graphs we study the case of pairs competition. Assuming that all genotypes have the same shape of the dose-response curves following the function $f_{\boldsymbol{\sigma}}(x)$, but differing parameters $r_{\boldsymbol{\sigma}}$ and $m_{\boldsymbol{\sigma}}$, it is evident that the role of the fittest between any two neighboring genotypes $\boldsymbol{\sigma}$ and $\boldsymbol{\sigma}^{+j}$ connected by an edge on the landscape is exchanged once the two related curves intersect at $x^*_{\boldsymbol{\sigma}}$. Assuming at $x = 0$ that $r_{\boldsymbol{\sigma}} > r_{\boldsymbol{\sigma}^{+j}}$, the intersection point (IP) will be given by

$$x^*_{\boldsymbol{\sigma},+j} = m_{\boldsymbol{\sigma}} \left[\frac{1 - \frac{r_{\boldsymbol{\sigma}+j}}{r_{\boldsymbol{\sigma}}}}{\frac{r_{\boldsymbol{\sigma}+j}}{r_{\boldsymbol{\sigma}}} - (\frac{m_{\boldsymbol{\sigma}}}{m_{\boldsymbol{\sigma}+j}})^{\alpha}} \right]^{\frac{1}{\alpha}}, \tag{6}$$

where it marks the transition between two fitness regimes

$$f_{\boldsymbol{\sigma}} > f_{\boldsymbol{\sigma}^{+j}} \quad \text{for} \quad x < x^*_{\boldsymbol{\sigma},+j} \tag{7}$$

and

$$f_{\boldsymbol{\sigma}} < f_{\boldsymbol{\sigma}^{+j}} \quad \text{for} \quad x > x^*_{\boldsymbol{\sigma},+j}. \tag{8}$$

In the context of the multiplicative growth of the fitness function parameters in the TIL model, the intersection points (IPs) reduce to

$$x^*_{\boldsymbol{\sigma},+j} = m_{\boldsymbol{\sigma}} \left[\frac{1 - r_j}{r_j - (\frac{1}{m_j})^{\alpha}} \right]^{\frac{1}{\alpha}}. \tag{9}$$

For the intersection to exist between the pair $\boldsymbol{\sigma}$ and $\boldsymbol{\sigma}^{+j}$, the Hill condition has to be satisfied

$$r_j m_j^{\alpha} > 1, \quad i = 1, 2, ..., L. \tag{10}$$

Otherwise, the mutant genotype equipped with mutation j will never be advantageous.

Next, unique properties to $r_{\boldsymbol{\sigma}}$ and $m_{\boldsymbol{\sigma}}$ are introduced, producing unique fitness landscapes. For reasons which will be made clear later, the mentioned parameters and the variable x are transformed to the logarithmic scale:

$$\chi = \ln x, \quad u_{\boldsymbol{\sigma}} = -\ln r_{\boldsymbol{\sigma}}, \quad v_{\boldsymbol{\sigma}} = \ln m_{\boldsymbol{\sigma}}. \tag{11}$$

Equations (3) and (6) are rewritten as

$$f_{\boldsymbol{\sigma}}(\chi) = \frac{e^{-(u_{\boldsymbol{\sigma}})}}{1 + (e^{\chi - v_{\boldsymbol{\sigma}}})^{\alpha}} \tag{12}$$

and

$$\chi^*_{\boldsymbol{\sigma},+j} = v_{\boldsymbol{\sigma}} + \frac{1}{\alpha} \ln \left(\frac{1 - e^{-(u_{\boldsymbol{\sigma}+j} - u_{\boldsymbol{\sigma}})}}{e^{-(u_{\boldsymbol{\sigma}+j} - u_{\boldsymbol{\sigma}})} - e^{-\alpha(v_{\boldsymbol{\sigma}+j} - v_{\boldsymbol{\sigma}})}} \right). \tag{13}$$

2.1.1 TIL Accessibility Property

The TIL landscapes show a unique high accessibility of peaks, where each peak is fully accessible from all genotypes of a subset of its mutations (subsets) and genotypes with additional mutations (super-sets). In [8], this unique accessibility was proven based on the fact that IPs, defined by placing a mutation j into different backgrounds in eq. (9), are ordered following the product $(\prod_{i \in I^+} m_i)$ or in the logarithmic scale the sum $(\sum_{i \in I^+} v_i)$, such that

$$\chi^*_{\boldsymbol{\sigma},+j} > \chi^*_{\boldsymbol{\sigma}^{-i},+j}, \tag{14}$$

for $j \in I^-$ and $i \in I^+$. Two major outcomes of this property are the accessibility of each peak from the wild type and the full accessibility of the full mutant once it becomes a peak.

We define rank orders of fitness that break the TIL accessibility property as *forbidden orders*. Given the definition of the accessibility property they arise when a genotype is fitter than its respective subset (super-set) of genotypes lacking a single mutation (having an additional mutation), but not fitter than the subsets (super-sets) of its respective subset (super-set). An example of a forbidden order in a two loci system would be $(00 > 11 > 10 > 01)$. One can avoid the rise of such orders by ensuring that all IPs are ordered with respect to the size of the mutational background for a particular new mutation j.

2.1.2 TIL Ruggedness

Ruggedness refers to the number of peaks a landscape displays. A single-peaked landscape is referred to as smooth, whereas multiple peaks make the landscape rugged. The TIL model is characterized by smooth landscapes in extreme conditions such as the absence of antibiotics and high concentration

of antibiotics. In between, the model exhibits ruggedness where more than one peak can carry evolution.

Note that smoothness in fitness landscapes facilitates selection of the fittest [5]. Still, the TIL model shows that a smooth landscape can evolve from a state of ruggedness and vice versa. Moreover, the model shows that ruggedness could be accompanied by high accessibility. Ruggedness and accessibility—two properties that seem to contradict each other were actually observed together in recent experimental setting [14]. The TIL model achieves this duality by ensuring that peaks do not fall in the subsets or super-sets of each other. In [15], it was shown that by satisfying this TIL accessibility condition, an upper bound on the number of peaks can be derived, which differs from the maximum number of peaks in an unconstrained landscape only by a polynomial factor.

2.2 Epistasis

To start with, we will define epistasis as the deviation from the additive picture (in the logarithmic scale). For an effect given by a quantity y_i introduced by a single mutation, the non-epistatic collective quantity of n mutations will be simply $y^0_{\boldsymbol{\sigma}} = \sum_{i \in I^+} y_i$, assuming no interactions between mutations. Epistasis in this context will be the difference between the interactions dependent quantity $y_{\boldsymbol{\sigma}}$ and the non-epistatic quantity:

$$\epsilon = y_{\boldsymbol{\sigma}} - \sum_{i \in I^+} y_i. \tag{15}$$

Negative epistasis implies that the epistatic quantity grows more slowly than the additive quantity, while positive epistasis implies the opposite. Both indicate interactions between mutations that affect the magnitude of the collective effect. Notice here that the TIL model is epsitasis-free in the parameters of fitness, however as the fitness depends non-linearly on these parameters it is still expected to show epistasis.

2.2.1 Submodularity Indicates TIL Accessibility

In the context of the TIL model, it was found that TIL orderings are always preserved in the case of negative epistasis [8]. Dominant negative epistasis interactions between any genotype and its subset of genotypes is known as

Universal Negative Epistasis (UNE) [15]. In a fitness model, TIL accessibility can be achieved by the choice of a fitness function that (itself or a monotonic transformation of this function) ensures UNE,

$$f(\boldsymbol{\sigma} \cup j) - f(\boldsymbol{\sigma}) \leq f(\boldsymbol{\sigma'} \cup j) - f(\boldsymbol{\sigma'}) \tag{16}$$

where $\boldsymbol{\sigma'} \subset \boldsymbol{\sigma}$. It was proven in [15] that UNE is guaranteed if pairwise negative epistasis between neighboring genotypes holds ($\boldsymbol{\sigma'} = \boldsymbol{\sigma}^{-i}$). Here, it can be proven that UNE is preserved when taking the logarithm of the TIL fitness function.

Submodularity is a property of set functions equivalent to UNE. A set function is submodular if an increase in the input sets leads to a shrinking growth in the output, a phenomenon commonly referred to as a *diminishing returns* growth.

2.2.2 Sign Epistasis

In the context of fitness, if mutations are beneficial in one genetic background but deleterious in another then it is said that the landscape displays sign epistasis. Sign epistasis is a feature of intermediate concentrations in the TIL model, where the transition of the fittest from one layer to the next is gradual. However, sign epistasis that dominates over a wide range of concentrations can occur when strong magnitude epistasis is present in some backgrounds and not in others. Such background dependence of epistasis is of interest in this work.

Sign epistasis could be seen as a source of TIL accessibility breaking, where deleterious effects of mutations in certain backgrounds can render some peaks inaccessible from their full subsets or super-sets.

In order to understand how epistasis in the parameters of the fitness function could alter the TIL picture and impact accessibility and ruggedness, Chapters 4 and 5 will explore a simple case of diminishing returns epistasis in these parameters. The motivation to introduce epistasis in the parameters is based on experimental results presented in Chapter 3.

3 Experimental Landscapes of β-Lactam Resistance

Tradeoff-Induced Landscapes (TIL) [8] is a mathematical model that was motivated by antibiotic dose-response curves of resistance of *Escherichia coli* in ciprofloxacin. The model describes evolution in a changing environment through adaptation-cost tradeoff (Fig. 1). It also assumes a simplified scenario with negligible interactions between mutations, where only weak epistasis is typically present—an assumption that requires further empirical validation.

Recent experimental data of evolution of *E. coli* in the context of $\beta-lactam$ resistance are available, which can be used to test the model [16]. How accurate are the assumptions on which the model is based? Is the model a good description of empirical outcomes in the context of other antibiotics? This chapter aims to analyze the available data to address these questions.

3.1 Data Overview

The dataset was obtained from the pre-print [16]. The experiment was performed on engineered DH5-α *E. coli* strains provided by the Weinreich Lab [17] using a gradient of Cefotaxime. These genotypes represent the full landscape of all possible combinations of four point mutations on the β-lactamase gene. Each point mutation individually increases the resistance of *E.coli* to the β-lactam antibiotic Cefotaxime.

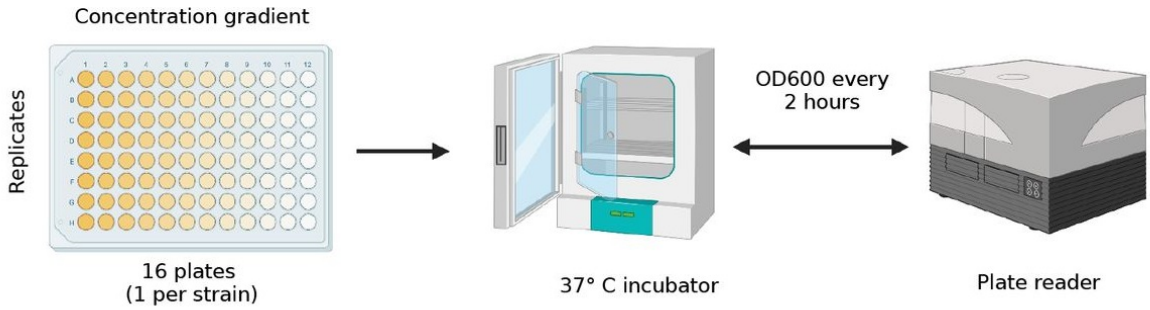

Figure 3: Experiment setup overview [16].

After incubating the strains overnight, the experiment was performed on 16 plates, each corresponding to a single genotype. In each plate, 10 columns

contained a gradient of 10 concentrations prepared using a 5-fold cefotaxime dilution scheme. One column was antibiotic-free, and another column was culture-free, serving as a control. The experiment was performed for each genotype with eight replicates. The growth of the replicates was recorded over 17 hours, with optical density readings taken every 1.5 hours allowing for a resolution of 9 data points per replicate (Fig. 3).

3.1.1 Background Noise Elimination

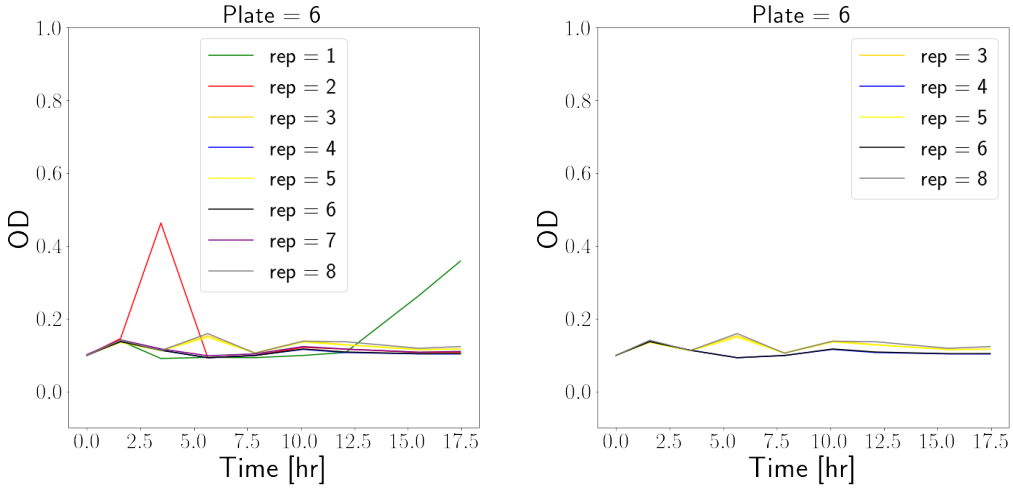

(a) (b)

Figure 4: Outliers in the background noise replicates 1, 2 and 7 in (a) were eliminated in (b). The point-wise average of the background noise was then subtracted from the raw data.

To minimize the influence of instrumental errors in the results, the background noise was quantified and eliminated. Investigating the background column data from the control column in each plate, apparent growth in culture free wells and single point irregular high readings were detected indicating contamination and other sources of irregular errors. These irregularities in the background data (Fig. 4a) were identified by detecting outliers using Tukey's fences:

$$OD_{\text{outlier}} \geq Q_3 + kQ, \tag{17}$$

where Q_i is the ith quartile among OD readings of replicates at a single time

point and Q is the interquartile range indicating the spread in the middle half, given by the difference between Q_1 and Q_3. The coefficient k is usually taken between 1.5 and 3, in this case chosen to be 2. Every background replicate with a single time point outlier was eliminated (Fig. 4b). After filtering outliers, the average background noise was identified at 0.1327 in OD units.

Background data was found to be biased towards higher or lower values across different plates and time points. Hence, background noise elimination was done point-wise by subtracting the average among control replicates from raw data at each time point for each plate following outlier removal.

3.1.2 Raw Data Outliers

Raw growth data was still showing some irregularities that could have resulted from human or instrumental errors rather than the background noise (Fig. 5). Some replicates started growing from an OD above 0.1, the threshold below which the culture is considered dead, which indicates that the culture started to grow before starting the experiment or a potential dilution failure (replicates 2,3,4,5,6,7 and 8 in Figure 5a and replicates 5,6 and 7 in Figure 5b). Other replicates showed sharp increase in OD for a single time point (replicate 4 in Fig. 5c). These were identified as extreme outliers and were systematically eliminated using Tukey's fences in eq. (17) setting the coefficient k to 40. Visual examination of the data showed this upper limit to exclude the irregular replicates. Finding outliers was tricky as the growth curves tend to fluctuate sharply. In order to avoid eliminating valid growth curves, only extreme outliers were eliminated. Other outliers resulting from contamination or a dilution failure that passed through the previous filters were manually eliminated (replicate 1 in Fig. 5d).

3.1.3 Eliminating Dead Replicas

Dead strains were identified given the last five data points. If two or more readings among these were below the threshold of $0.09237 \approx 0.1$ in OD units, the replicate's growth trajectory is set to zero.

The threshold is a mean of the last five data points when the maximum OD yield is in the 5.5 early hours or among the four first data points, indicating the dying out of growth for later time points in the experiment (Fig. 6).

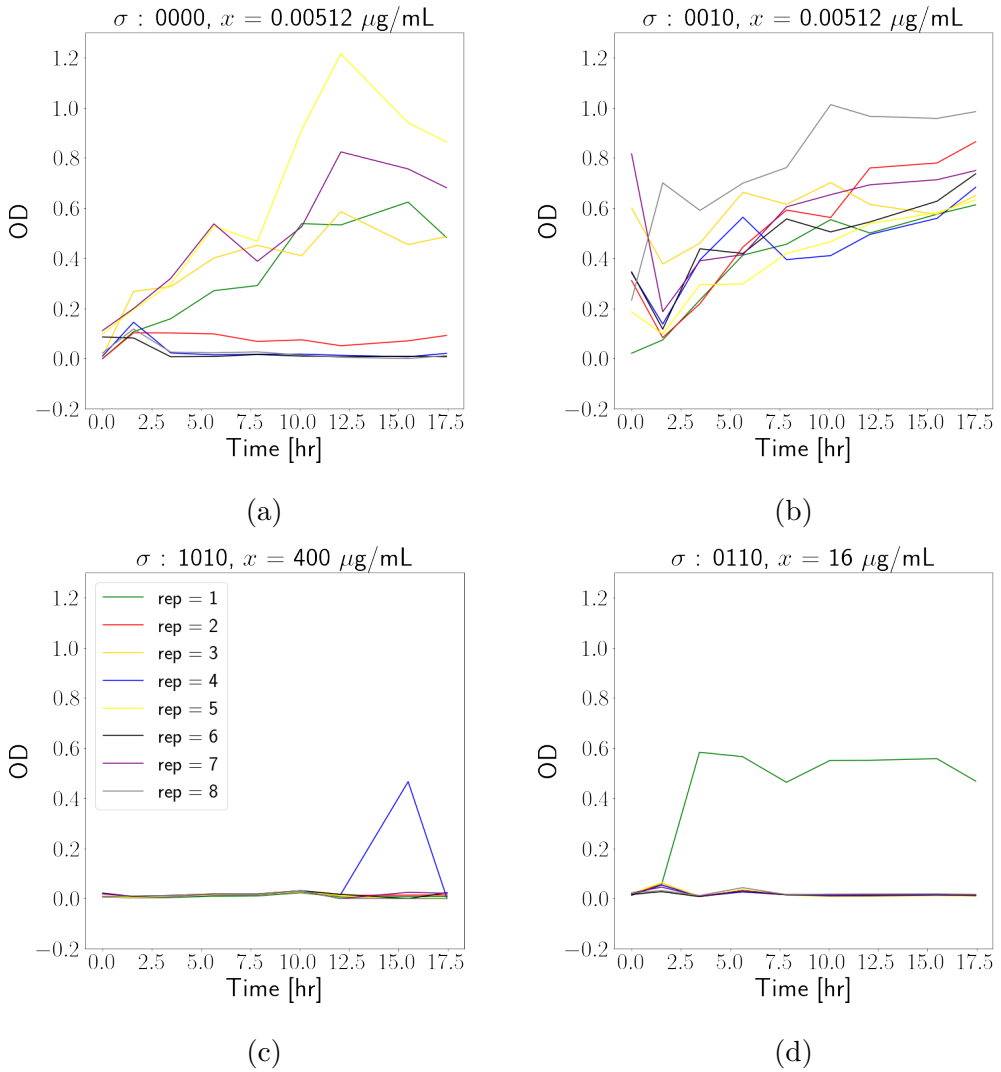

Figure 5: Replicas with outlying behavior in the raw data. Outliers could be identified as initial growth above 0.1 in OD units in replicates 2,3,4,5,6,7 and 8 in (a) and replicates 5,6 and 7 in (b), sharp increase in a single time point in replicate 4 in (c) and growth due to probable contamination in replicate 1 in (d).

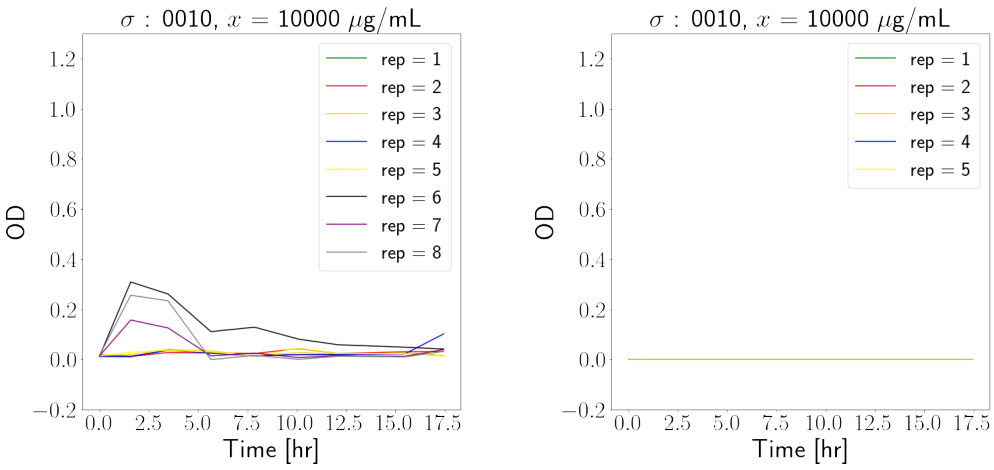

(a) (b)

Figure 6: Replicas that eventually die (a) were set to zero growth (b).

3.2 A Suitable Fitness Measure

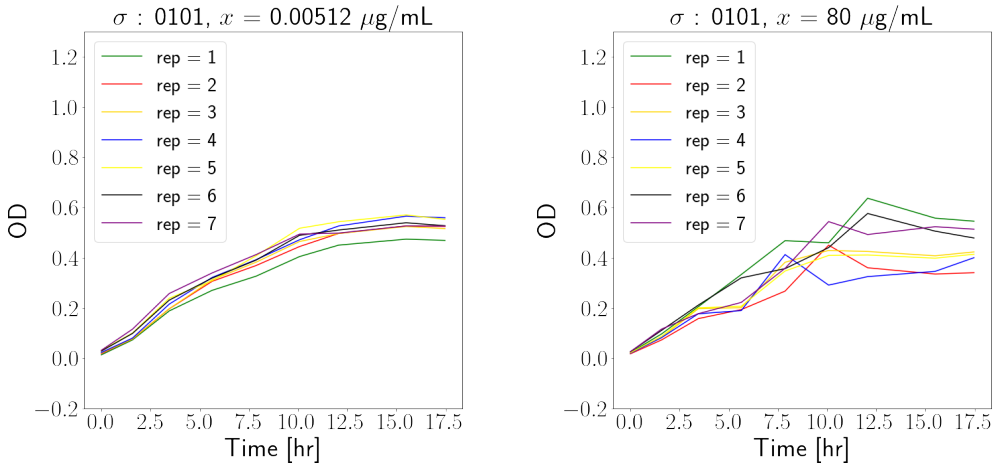

(a) (b)

Figure 7: Phases of growth in the OD curves. Growth curves change behavior as the concentration increases, identifying three phases of growth. Stable growth at low concentrations is shown in (a). Fluctuating phase at intermediate concentrations is shown in (b), where replicates show unsteady growth pattern that diverge from one another. The third phase is the death phase was shown in Figure 6.

3.2.1 Phases of Growth

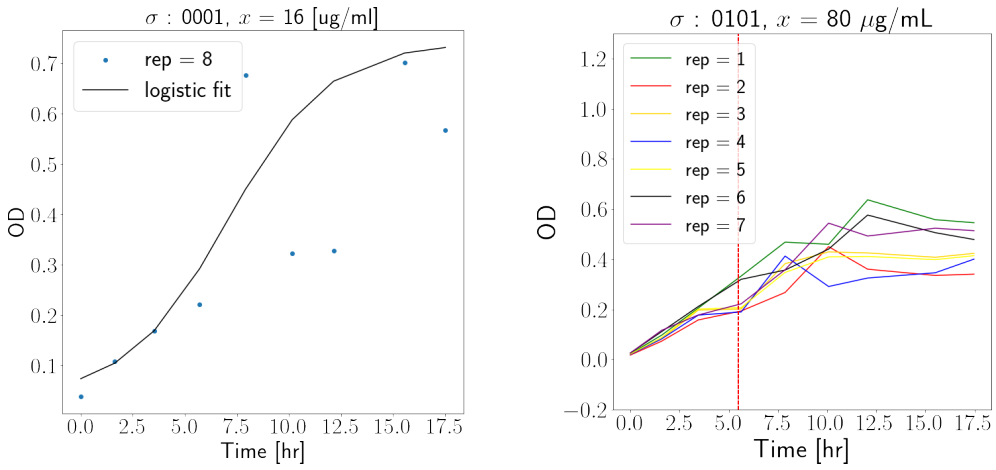

(a) (b)

Figure 8: An example of a poor logistic fit of the growth curve in the fluctuating phase shown in (a). Growth curve cutoff is shown in (b). The section of the growth curve defined as steady is up to the red mark.

As discussed in the previous sections, the raw data required few steps of filtering to keep the observed growth behavior reasonable. Investigating the growth behavior, three distinct phases were identified across all genotypes (Fig 7):

1. A stable phase: At low concentrations nearly all replicates follow the same growth trajectory.

2. A fluctuating phase: At sub-MIC (minimum inhibitory concentration or the lowest concentration that inhibits the growth of a given genotype) the genotypes show unsteady growth patterns that diverge among replicates.

3. A death phase: Beyond MIC the growth decays and the culture dies.

3.2.2 AUC or Growth Rate?

Given the growth curves, fitness can be identified through one of two measures. The first measure can be found by extracting the growth rate (R) by fitting the growth curve to a logistic function. The second measure is the mean biomass achieved by the population, approximated by the area under the growth curve (AUC).

When estimating R, the fluctuating phase marked by the unsteady growth of replicates at sub-MIC concentrations led to poor logistic function fits. The following logistic function was used following the choice in [16]:

$$OD = OD_0 + \frac{OD_{\max}}{1 + \exp[\frac{4R}{OD_{\max}}(t_{\text{lag}} - t) + 2]}, \tag{18}$$

where $OD_{\max}$ is the maximum yield of optical density and t_{lag} is the lag time before exponential growth, parameterized by the rate R, is activated [18].

The poor logistic function fits had unreasonable error levels. When considering the fitted growth rate R as a measure of fitness, the fits contributed to apparent fitness at intermediate concentrations that is higher than the fitness associated with stable growth at lower concentrations. This results in irregular behavior in the dose-response curves with high error margins during fitting. As a consequence, fitting the growth curves was not a reliable option for determining fitness (Fig. 8a).

Instead, the first few hours of growth before fluctuations dominate presented a more robust, systematic behavior through all concentrations. Therefore, a cutoff after a few hours of growth was introduced. This part of the growth curve will be referred to as the steady part in the following discussions (Fig. 8b). Taking the steady part of the growth curves into account, only 5.5 hours of growth were considered, equivalent to only four data points in the current experiment (Fig. 8b). One can still attempt to find the maximum slope among the few data points left to approximate R, however, the AUC was found to be more robust in terms of considering more data points and hence being less sensitive than the growth rate to single point errors. More detailed discussion is provided in the supplementary material.

For comparison, the same following analysis was done employing the AUC of the entire growth and the main results are summarized in the supplementary material.

3.3 Results

Using the averaged AUC of the steady parts of the growth curves as a fitness measure, the dose-response curves were fitted to the Hill function in eq. (12), where the null-fitness (u) and the IC_{50} (v), both normalized with respect to the wild type, were extracted (Fig. 9) for a chosen Hill coefficient of $\alpha = 4$.

The Hill coefficient was chosen as the smallest possible value that maintained tolerable levels of error. The steepness of the dose-response curves is quite high here, reflecting the low resolution of the experiment where the gradual loss of fitness cannot be observed.

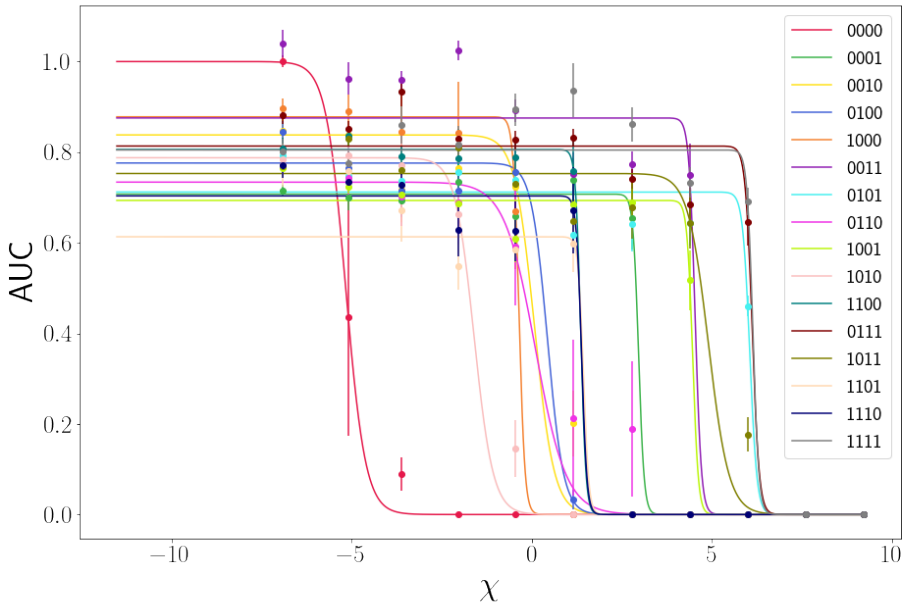

Figure 9: Solid lines show the fitted dose-response curves. The average of the experimentally obtained data is shown in the scatter. The AUC was normalized with respect to the wild type's null-fitness. χ here is given in units of $\log(mg/ml)$.

3.3.1 Tradeoff Behavior

When investigating the trend of fitness in the dose-response curves averaged over the number of mutations, tradeoff are apparent (Fig. 10a). On average, higher the accumulated number of mutations, weaker the fitness at low concentration but the population dies out at a later stage.

Tradeoff between the null-fitness (u) and IC_{50} (v) can be directly tested by finding whether these two quantities anti-correlate across genotypes. In Figure 10b, weak anti-correlation is observed with a weak negative slope between the two quantities (-0.012) indicating weak tradeoff. The weak tradeoff trend is

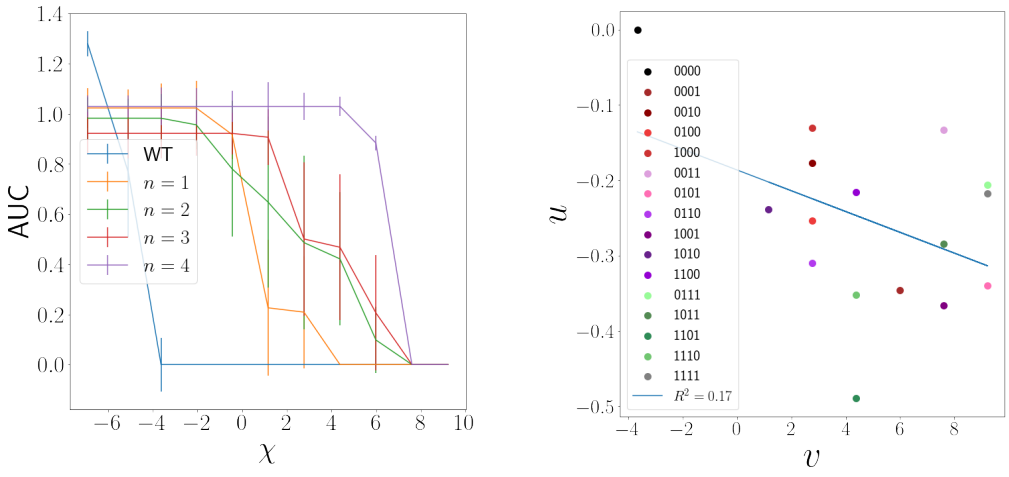

(a) (b)

Figure 10: Dose-response curves averaged over number of mutations in (a). Tradeoff trend between null-fitness u and IC_50 v in (b).

attributed to epistatic interactions between mutations along with the low cost of some mutations as shown later.

3.3.2 Epistasis

Here, epistasis patterns in the parameters $(u_{\boldsymbol{\sigma}}, v_{\boldsymbol{\sigma}})$ and in the fitness $(f_{\boldsymbol{\sigma}})$ is studied. To quantify epistasis, the non-epistatic value assumed for a parameter is compared to its experimentally obtained value. For a parameter $x_{\boldsymbol{\sigma}}$ of a genotype $\boldsymbol{\sigma}$, the epistasis is found through the definition in eq. (15).

The TIL model was motivated by a dominantly weak epistasis trend detected in the null-fitness and IC_{50} for *E. coli* growth in ciprofloxacin [8, 19], an antibiotic with a different mechanism from $\beta-$lactam antibiotics. In the current results, the epistasis trend in the parameters is notably strong. Null-fitness r is found to display an increasing positive epistasis (which translates to a growing negative epistasis in the cost u), the amount of epistasis varies among mutants, but is mainly responsible for the slow decrease in the null-fitness compared with the growth in the number of mutations. For example, the full mutant had lower mutational cost than the average triple mutants (Fig. 11), indicating that the cost of mutations is not necessarily universal.

On the other hand, IC_{50} displays sharp negative epistasis that grows with

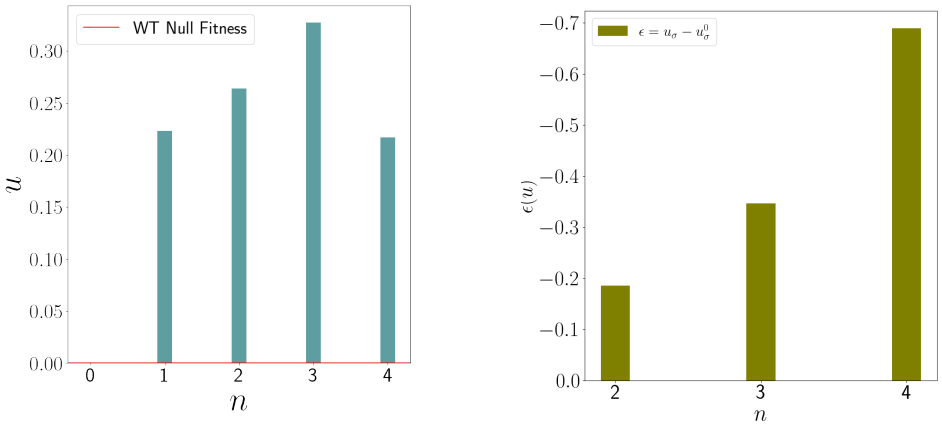

(a) (b)

Figure 11: The average cost of mutation trend across number of mutations (a) and the average epistasis in null-fitness against number of mutations (b).

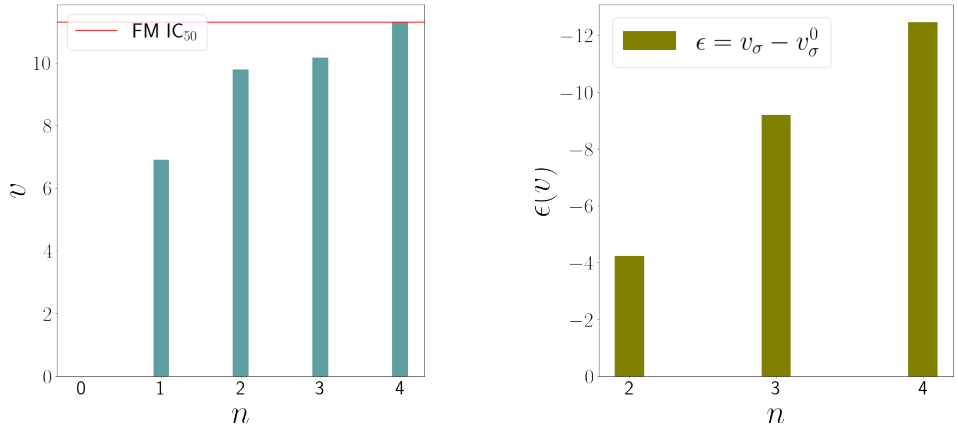

(a) (b)

Figure 12: The average IC_{50} trend across number of mutations (a) and the average epistasis in IC_{50} (b).

number of mutations, a feature indicating diminishing returns epistasis or reduction of benefit in an advantageous background. This trend keeps IC_{50} around 50 % lower than the levels predicted by the TIL model and makes resistance comparable for genotypes with two, three, and four mutations in some cases (Fig. 12).

As a general observation, the data shows a *global* trend of intrinsic epistasis, where gene-gene interactions govern the impact of mutations on the null-fitness and IC_{50} independent of the environment; the null-fitness (IC_{50})

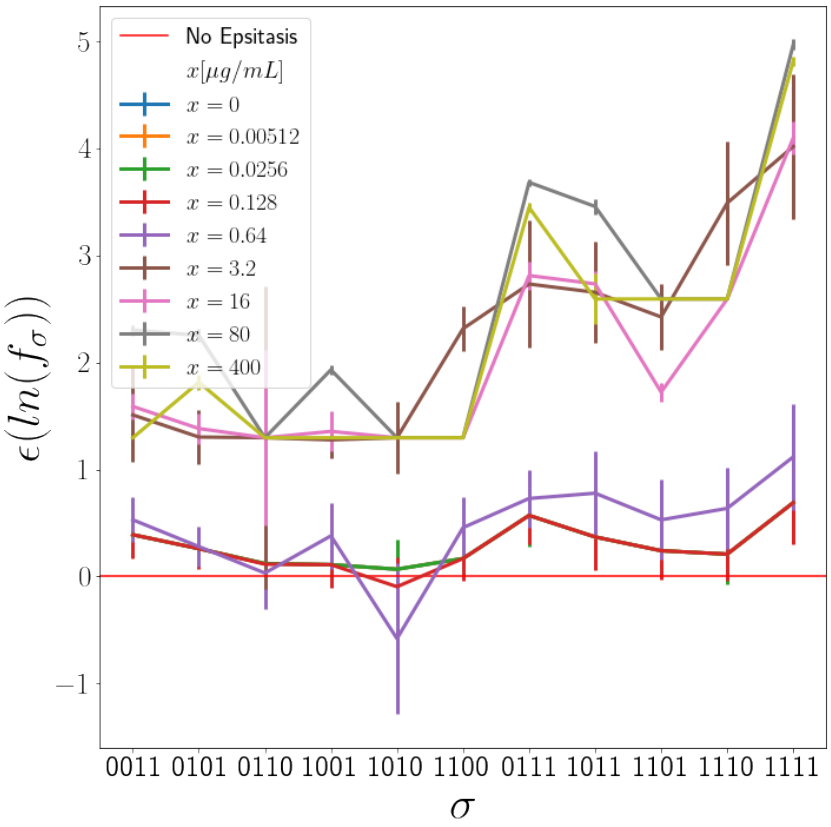

Figure 13: The epistasis in fitness for genotypes across different concentrations, the epistasis was computed using eq. 15. Epistasis detected in the fitness is dominantly positive. Notice that, at low concentrations epistasis values (blue, orange, green and red) overlap.

seems to always drop (increase) as mutations accumulate at a rate slower than the assumed multiplicative way by the TIL model.

In terms of fitness, the results show dominant positive epistasis (Fig. 13). This non-trivial result shows that magnitude epistasis in the fitness parameters can increase adaptivity. The fitness of dead strains was approximated by the minimum growth detected and not set to zero. The large jump in epistasis values for concentrations where most single mutants are considered dead (starting at 3.4 μg/ml) creates two different regimes of epistasis. At low concentrations the epistasis is weakly positive, while at high concentrations the epistasis increases with the number of mutations. Note the overlap of epistasis values at low concentrations, where the fitted fitness values tend to be constant

for concentrations below the MIC.

3.3.3 Fitness Landscape, Accessibility and Ruggedness

The fitness landscapes (Fig. 14) display a gradual increase in the number of mutations for peaks as the concentration is increased, which is a feature expected in the TIL model. All peaks are accessible from the wild type in the presence of antibiotics, another feature predicted by the model. However, the fitness vs number of mutations trend is complex beyond the peaks, with epistasis resulting in few mutations being deleterious in their background (subset of mutations) at high concentrations. For example, the genotype "1010" dies before its respective background.

The TIL model assumes a smooth landscape at the extreme values of the environmental variable. The intermediate transitioning phase between the two smooth landscapes is assumed to be rugged and dominated by sign epistasis. The current results show that the landscapes start with a rugged landscape at low concentrations and transition to a relatively smooth one at high concentrations with a single fitness maximum and a lower degree of sign epistasis. At high concentrations, many genotypes are dead and the few resistant genotypes serve as a basin of attraction for evolution, the landscape will tend almost always to be smooth.

The genotype "0011" exhbits an interesting behavior, where it remains a peak for a wide range of concentrations. The landscape displays constant ruggedness at low concentrations with two peaks one of which is always the genotype "0011". At high concentrations, many genotypes are taken to be dead and only one peak is possible to maintain. The system under study is small. Therefore, the asymptotic ruggedness behavior of landscapes in the TIL model should not be expected.

3.3.4 IC_{50} Landscape and the Accessibility of the Fittest

The fitness landscape in Figure 14 shows that high resistance is associated with a higher number of mutations. However, it reflects occasional deleterious effects of some mutations where the mutant carrying them might die before its subset (genotype 1010 is an example).

Nonetheless, the full mutant has a high level of accessibility with 14 out of

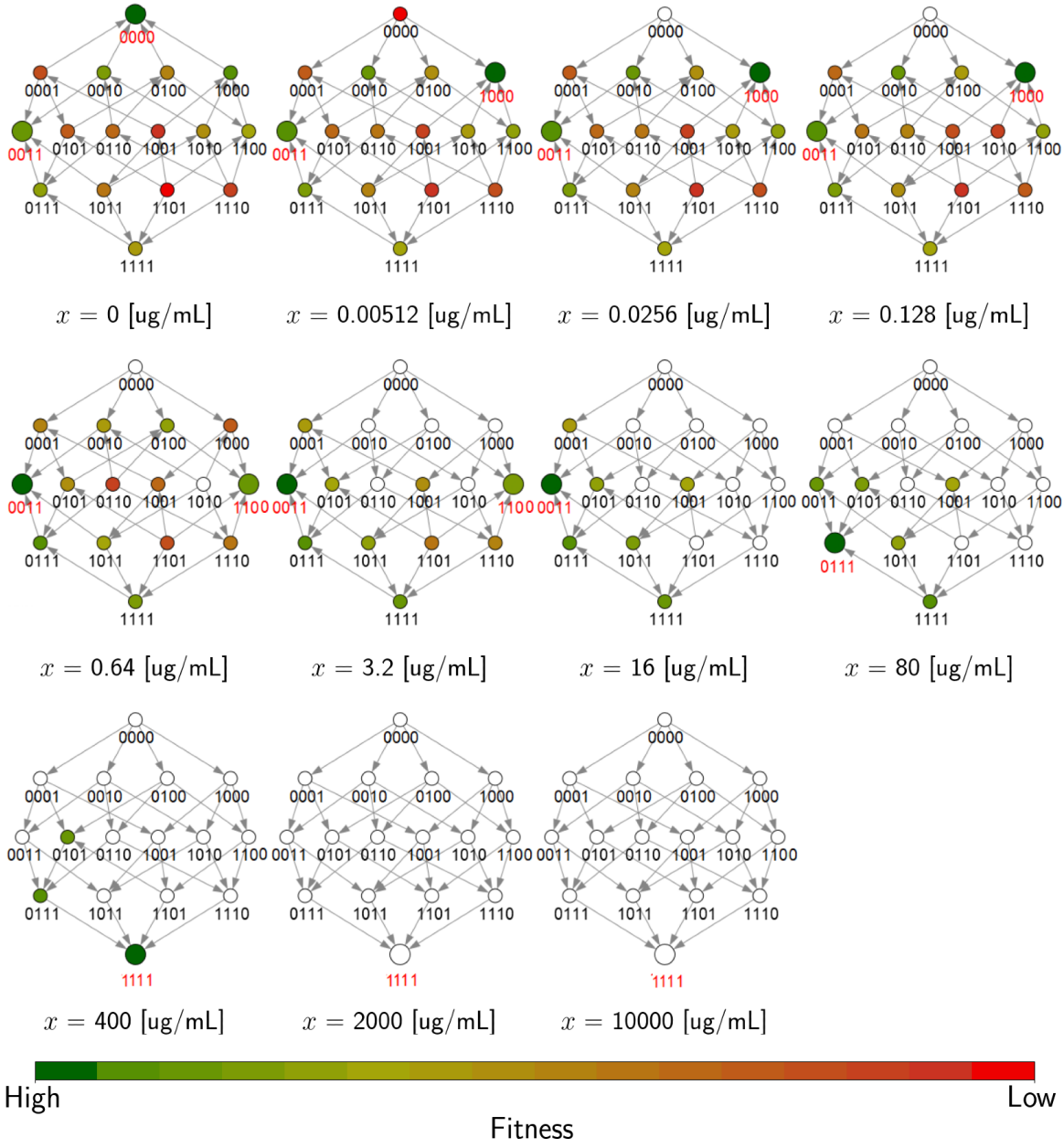

Figure 14: Full landscapes in a changing environment of antibiotics, the color of the vertex identifies the genotype's fitness on a scale of (high - low). White nodes are genotypes that are assumed dead at this concentration, and the nodes of bigger size and labeled red are peaks.

24 direct paths from the wild type being accessible in the fitted IC_{50} landscape (Fig. 15a). This result contradicts the results on evolution of *E. coli* in Cefotaxime by Weinreich et al., where only a few accessible paths were reported. The results from 2006 are for a system of five mutations including the current four with an additional regulatory mutation [17].

In Weinreich et al., the accessibility of the fittest was defined through an alternative measure of resistance, which is the MIC. The maximum inhibitory concentration (MIC) is the highest concentration at which the genotype was experimentally viable. In the current raw data, different genotypes appear to have the same MIC values as well. This observation is due to the discrete nature of the experiment and the intrinsic logarithmic scaling of the concentrations in the dilution scheme. The MIC landscape of the current dataset is shown in Figure 15b for comparison, where we also find multiple genotypes to die at the same concentration.

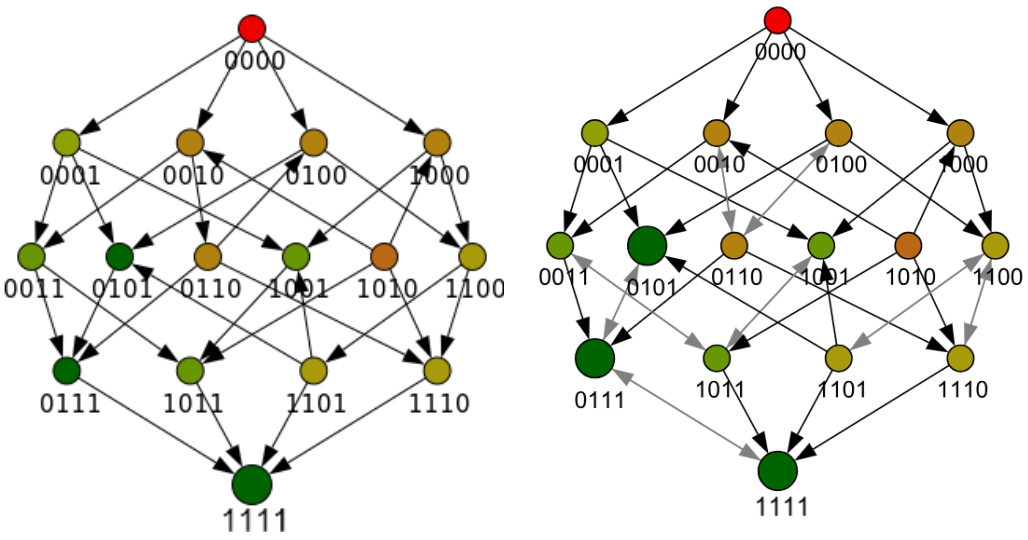

Figure 15: A comparison between the IC_{50} and the MIC landscapes. The IC_{50} values in (a) were obtained through the fitted m values in eq. (3), while in (b) the MIC is the last concentration in the experimental setting where the strain is viable. In (b), neutral transitions are shown in bidirectional arrows colored grey. It is notable that the full mutant is accessible in the IC_{50} landscape through 14 paths while considering the neutral mutants deleterious in the MIC landscape means that the full mutant in inaccessible from the wild type.

In a strong-selection weak-mutation regime of evolution, which is assumed in this case, neutrality blocks evolution, where neutral mutations have a very low probability of fixing. Under this assumption, rejecting all paths of apparent neutral mutations Weinreich et al. found out that 18 out of 120 evolutionary trajectories were only accessible from the wild type to the full mutant. Applying the same approach, the MIC landscape in Figure 15b is entirely blocked, which primarily indicates the low resolution of the experiment.

The assumption that genotypes dying at the same experimental dose are of equivalent resistance in the context of a discrete exponential scale is not accurate. In order to solve this issue, Weinreich et al. randomized the ambiguous MIC values and found that 39 out of 120 trajectories became accessible. As the general trend is of mutations being beneficial in most backgrounds, the randomization approach is not the best approximation where a preference for the mutants should be assumed. This leads to the conclusion that the full mutant in the context of evolution of *E. coli* in Cefotaxime has higher accessibility than Weinreich et al. concluded, a finding emphasised by the results of this experiment.

3.3.5 Dose-Response Curves Intersection

An important indication of the landscape dynamics is the patterns intersection points (IPs). The TIL model accessibility is ensured whenever dose-response curves of all genotypes and their respective backgrounds intersect at most once allowing for a gradual fitness rank-order change among neighboring genotypes and permitting the smooth evolution of the most resistant genotypes through various paths.

In order to understand the dynamics of fitness rank order change, the number of intersections between neighboring genotypes was counted. It was found that 17 out of 32 neighboring pairs of dose-response curves intersect once. Among the 15 remaining pairs, there were 9 mutants that were fitter than their background throughout the experiment protocol of concentrations.

The data in hand showed general preference of higher number of mutations at high concentrations where many arrows are leading directly to the full mutant. Although, some mutants were already fitter than their backgrounds in the absence of antibiotics, there is not a single case of switching order that

allowed a genotype to become fitter than any of its super-sets. Once a mutant is fitter than its background, it remains fitter for all higher concentrations. This emphasizes the effective advantage the mutations in most backgrounds bring, along with the presence of a cost preventing many mutants from being competitive in the absence of antibiotics but making them beneficial in the presence of antibiotic stress.

3.3.6 State Transition Graph

Evolutionary trajectories are best visualized by a state transition graph, assuming antibiotic concentration monotonically increases or decreases in a quasi-static manner. Quasi-static concentration change is slow enough that the population is allowed to fix after each concentration change. In a state transition graph, the transitions between peaks in a sequence of fitness landscapes are represented in a single graph [11].

The resulting state transition graph displays transitions among peaks as the stress of antibiotics is increased (Fig. 16). All peaks are reachable by greedy and non-greedy walks from the wild type. It is evident that as the concentration increases, a gradual increase in the number of mutations leads to the emergence of the most resistant genotype. The absence of a smooth landscape at low concentrations is illustrated in the descending state graph, where the walk starts from two different originating states, the full mutant "1111" and the double mutant "1100". The descending walk also has two different absorbing states, including the double mutant "0011", which is exceptionally fit and a peak throughout a wide range of concentrations and in the absence of antibiotics. The wild type is inaccessible from the full mutant as the concentration decreases in this structure. Reversibility is known to be driven by the cost of mutations, and as the cost of the current mutations tends to be low in some cases, this blocks the path to reverse evolution [20].

Results obtained in this chapter can be reproduced through the code posted on GitHub: (Beta–Lactam-evolution-experiment-data-analysis)

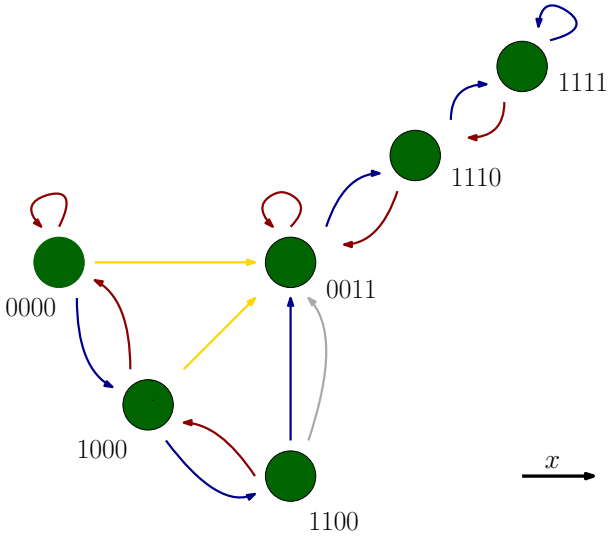

Figure 16: State transition graph showing transitions in the case of increasing concentration in blue and in the case of decreasing concentration in red considering greedy walks, whereas yellow and grey are respectively the increasing and the decreasing non-greedy walks. Greedy walks follow the path maximizing fitness in each step, while non-greedy walks follow a path with increasing fitness that doesn't necessarily maximize fitness. The order of the genotypes follows from left to right the order at which these peaks cease being one as the concentration is increased.

4 Deterministic Model of Magnitude Epistasis

One approach to understanding the experimental picture of evolution of resistance in Chapter 3 is by introducing magnitude epistasis to the framework of the TIL model. The approach of the TIL model describing fitness in a changing environment through genotype-specific parameters that display a tradeoff proved reasonable in the experiment analysis. Additionally, the TIL model lays the foundation to effectively explain the varying nature of epistasis in fitness in terms of the epistasis trend in either of the two tradeoff parameters depending on the regime of stress displayed by the environment. Environment dependence of epistasis in fitness has been reported in the literature [21].

In the framework of eq. (12), the null-fitness is presented by the cost parameter u. The positive epistasis in the null-fitness can be translated to diminishing returns epistasis in the cost. Hence, in the following discussion, diminishing returns epistasis will be introduced to both the cost and the resistance. Diminishing returns epistasis, a form of interaction between mutations where a mutation effect decreases as the background size to which it is added increases, is reported in evolution experiments of diverse levels of biological organisms [9, 10].

4.1 Magnitude Epistasis Introduced (TILME)

In order to properly define the genotype sequence for the purposes of this section, we define the vector $\boldsymbol{u}_L$, as the totally ordered set of the cost of mutations (the logarithmic transform of the inverse of the null-fitness) brought by L different mutations individually $U_L = \{u_i : 1 \leq i \leq L\}$,

$$\boldsymbol{u_L} = (U_L, <), \quad u_1 < u_2 < .. < u_L. \tag{19}$$

Now, we have an ordered vector of L different values from the smallest to the Largest. This vector will be used as a reference to label our L mutations. When referring to the mutation 1, it is the mutation with the smallest cost (largest null-fitness). Mutation 2 has of the second smallest cost and mutation L is the mutation with the largest cost value. This order will serve in later analysis.

Defining $\boldsymbol{\sigma}$, we will choose the mutation position on the sequence according to its label (order of $\boldsymbol{u}_L$)

$$\boldsymbol{\sigma} = (\sigma_1, \sigma_2, .., \sigma_i, ..\sigma_L). \tag{20}$$

One way to present diminishing returns epistasis is to make the contribution of a new mutation size-dependent by introducing an exponent,

$$u_{\boldsymbol{\sigma}} = (\sum_{i \in I^+} u_i)^{\mu},\ v_{\boldsymbol{\sigma}} = (\sum_{i \in I^+} v_i)^{\nu} \tag{21}$$

where for $0 < \mu < 1$ and $0 < \nu < 1$, the diminishing returns effect is achieved. Diminishing returns here have the effect of positive magnitude epistasis in null-fitness and negative magnitude epistasis in the IC_{50} (see eq. (11)).

Following the introduction of magnitude epistasis to the TIL model (TILME), our fitness and IPs will explicitly be written as:

$$f_{\boldsymbol{\sigma}}(x) = \frac{e^{-(\sum_{i \in I^+} u_i)^{\mu}}}{1 + (e^{\chi - (\sum_{i \in I^+} v_i)^{\nu}})^{\alpha}} \tag{22}$$

and

$$\chi^*_{\boldsymbol{\sigma},+j} = (\sum_{i \in I^+} v_i)^{\nu} + \frac{1}{\alpha} \ln \left(\frac{1 - e^{-((\sum_{i \in I^+} u_i + u_j)^{\mu} - (\sum_{i \in I^+} u_i)^{\mu})}}{e^{-((\sum_{i \in I^+} u_i + u_j)^{\mu} - (\sum_{i \in I^+} u_i)^{\mu})} - e^{-\alpha((\sum_{i \in I^+} v_i + v_j)^{\nu} - (\sum_{i \in I^+} v)^{\nu})}} \right), \tag{23}$$

where $j \in I^-$ and $i \in I^+$. The current experimental data was used to extract the values of μ and ν, results can be found in table 2 in the supplementary material.

In the context of diminishing returns epistasis, dose-response curves in eq. (22) become steeper as epistasis increases (μ and ν decrease). The lower ν and μ are, the faster fitness drops, and the lower the concentrations at which IPs between dose-response curves take place. Consequently, diminishing returns epistasis accelerates the loss of the advantage in mutant genotypes (Fig. 17) [22].

4.2 Evolution Condition

For advantageous mutations, the Hill condition in eq. (10) after applying magnitude epistasis translates to:

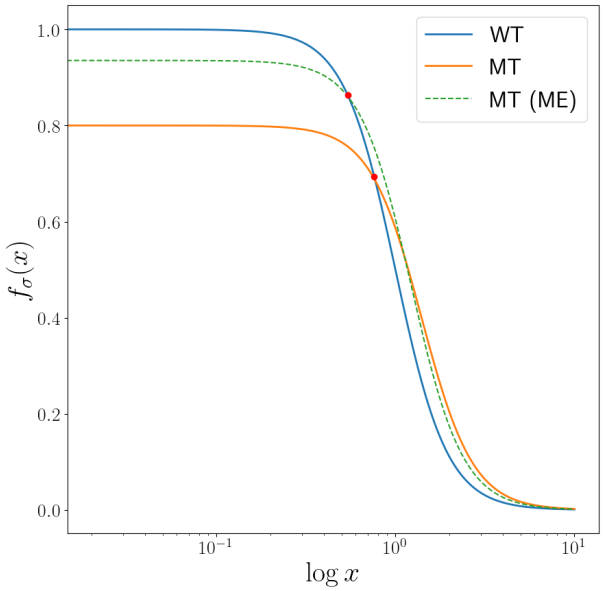

Figure 17: Diminishing returns epistasis has the effect of speeding the loss of advantage by enhancing the null-fitness of mutants while enforcing a steeper drop in fitness as concentration increases. The dashed curve for a mutant (MT) of $\mu = 0.3$ and $\nu = 0.6$ becomes fitter than the wild type (WT) at a concentration lower than the epistasis free case.

$$\alpha(\sum_{i\in I^+} v_i + v_j)^\nu - \alpha(\sum_{i\in I^+} v_i)^\nu > (\sum_{i\in I^+} u_i + u_j)^\mu - (\sum_{i\in I^+} u_i)^\mu \tag{24}$$

where $j \in I^-$. In the following we assume μ and ν to be constant for simplicity.

This condition ensures the intersection of dose-response curves and hence evolution. We will refer to both eq. (10) and eq. (24) as the evolution condition in the TIL and TILME models, respectively.

4.2.1 Evolution Condition of the Deterministic System

In a changing environment, a mutation will bring an evolutionary advantage at a given stress level or it might always be deleterious. In the TIL model, this depends on the background to which it is added. The background dependence complicates analytical and computational efforts to account for advantageous mutations as the system grows in the number of mutations L. To understand how magnitude epistasis restricts evolution, the simplest case of deterministic

evolution is investigated first, where all mutations have the same effect:

$$u_i = u, v_i = v. \tag{25}$$

The evolution condition simplifies to

$$\alpha v^\nu((n+1)^\nu - (n)^\nu) > u^\mu((n+1)^\mu - (n)^\mu), \tag{26}$$

rearranging,

$$\frac{((n+1)^\nu - (n)^\nu)}{((n+1)^\mu - (n)^\mu)} > \frac{u^\mu}{\alpha v^\nu}. \tag{27}$$

The LHS is strictly increasing if $\nu > \mu$ and strictly decreasing for $\mu > \nu$. This indicates that evolution is more likely to take place in the first case. In the second case, carrying more mutations is seen as a disadvantage because of the small gain in resistance at a relatively high cost.

For each case, it is straightforward to verify the possibility of evolution by studying the appropriate bound. In the case of $\nu > \mu$, evolution is guaranteed for arbitrary system size if

$$\alpha v^\nu > u^\mu. \tag{28}$$

On the other hand, if $\mu > \nu$, then one has to consider a more restricted condition dependent on L,

$$\alpha v^\nu \frac{(L^\nu - (L-1)^\nu)}{(L^\mu - (L-1)^\mu)} > u^\mu \tag{29}$$

which if satisfied, evolution is guaranteed for the full landscape.

Considering the limiting case of eq. (29) for LHS = RHS, one can find the shape of the bound for deterministic evolution. The deterministic bound is shown in Figure 18 in black, above which evolution is always guaranteed to occur if mutations have identical effect.

4.2.2 Locating the Experimental Data Regime

Next, we try to find intervals from which u_i and v_i could be sampled randomly allowing evolution. This regime is found to be independent of the size of the sampling interval, and has a fixed shape for a given system size L and a given epistasis level (μ and ν) (Fig. 18).

Let n be the number of mutations in $I^+(\boldsymbol{\sigma})$. To simplify the condition in eq. (24), two intervals are defined from which random variables u_i and v_i are

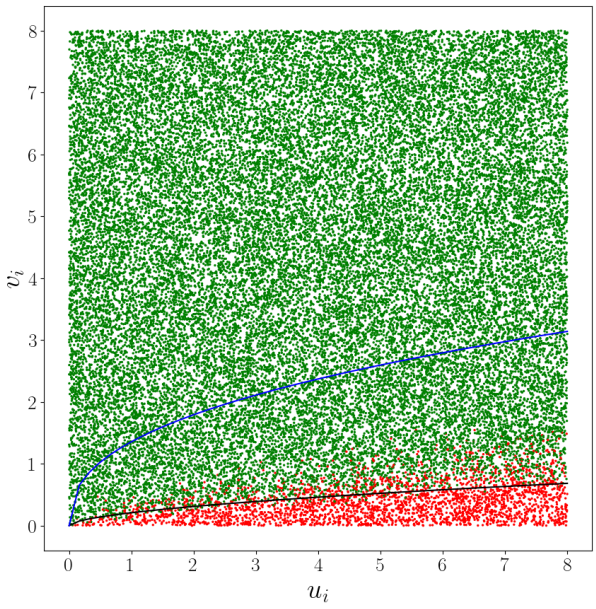

Figure 18: The parameters shown are sampled uniformly from the interval (0,8). Four parameter pairs (v_i, u_i) are sampled together representing four mutations, then evolution is tested in different background combinations representing all paths on a landscape. Parameters for mutations allowing for evolution in all possible backgrounds to take place are scattered in green, but whenever evolution is blocked in at least a single background they are scattered in red. The black line defines the deterministic bound for which $v_i = v$ and $u_i = u$, where above the line evolution deterministically takes place according to the limiting case of eq. (29). Whereas the blue line defines the boundary above which evolution is guaranteed sampling randomly from ranges that have $c = 8$ according to eq. (30). Here, $\mu = 0.4$ and $\nu = 0.7$.

sampled. The condition is then restricted to test intervals by considering the values minimizing the left-hand side and maximizing the right-hand side,

$$\alpha(n\max(v_i) + \min(v_i))^\nu - \alpha(n\max(v_i))^\nu > (n\min(u_i) + \max(u_i))^\mu - (n\min(u_i))^\mu. \quad (30)$$

Now a bound case for the stochastic picture exists taking the eq. in (30) assuming $v_{max} = c$, a constant, and $u_{min} = 0$ as two known limits. The variables of interest here are u_{max} and v_{min}, which have the following dependency:

$$v = \left(\frac{u^\mu}{\alpha} + (Lc)^\nu\right)^{1/\nu} - Lc, \tag{31}$$

defining the boundary above which evolution always takes place.

In Figure 18, u_i and v_i can be sampled from the part above the blue line (defined by eq. (31)) with absolute confidence in evolution regardless of the background. It is important to mention that eq. (31) defines the limiting case of absolute confidence, where evolution might take place for most sampled parameters from below the blue line. The parameter regime related to the experimental data in Table 1 is found to guarantee evolution.

4.3 TIL Accessibility Property in TILME

When evolution is guaranteed in landscapes ruled by diminishing returns epistasis, one can ask now whether the TIL accessibility still holds, allowing for highly accessible peaks in the landscapes. This question is mathematically equivalent to asking whether eq. (23) is always an increasing function upon adding a mutation j. This cannot be guaranteed for all choices of (v_j, u_j, μ, ν). Therefore, it is expected that the TIL accessibility property is not always satisfied.

4.3.1 Fitness Function Analysis

To develop an idea about the conditions under which accessibility breaking is expected, we will study the deterministic fitness function in the number of mutations n in the continuous limit,

$$f(n) = \frac{e^{-(nu)^\mu}}{1 + (e^{\chi - (nv)^\nu})^\alpha}. \tag{32}$$

Bear in mind that a monotonically increasing or decreasing function along with a strictly concave function will have peaks in a single layer which will be accessible from all other layers, guaranteeing the TIL accessibility property (Fig. 19).

In the following, we work with the logarithm of the fitness function ($\ln(f(n))$) for it to simplify the analysis.

The first derivative of the logarithm of eq. (32) is given by

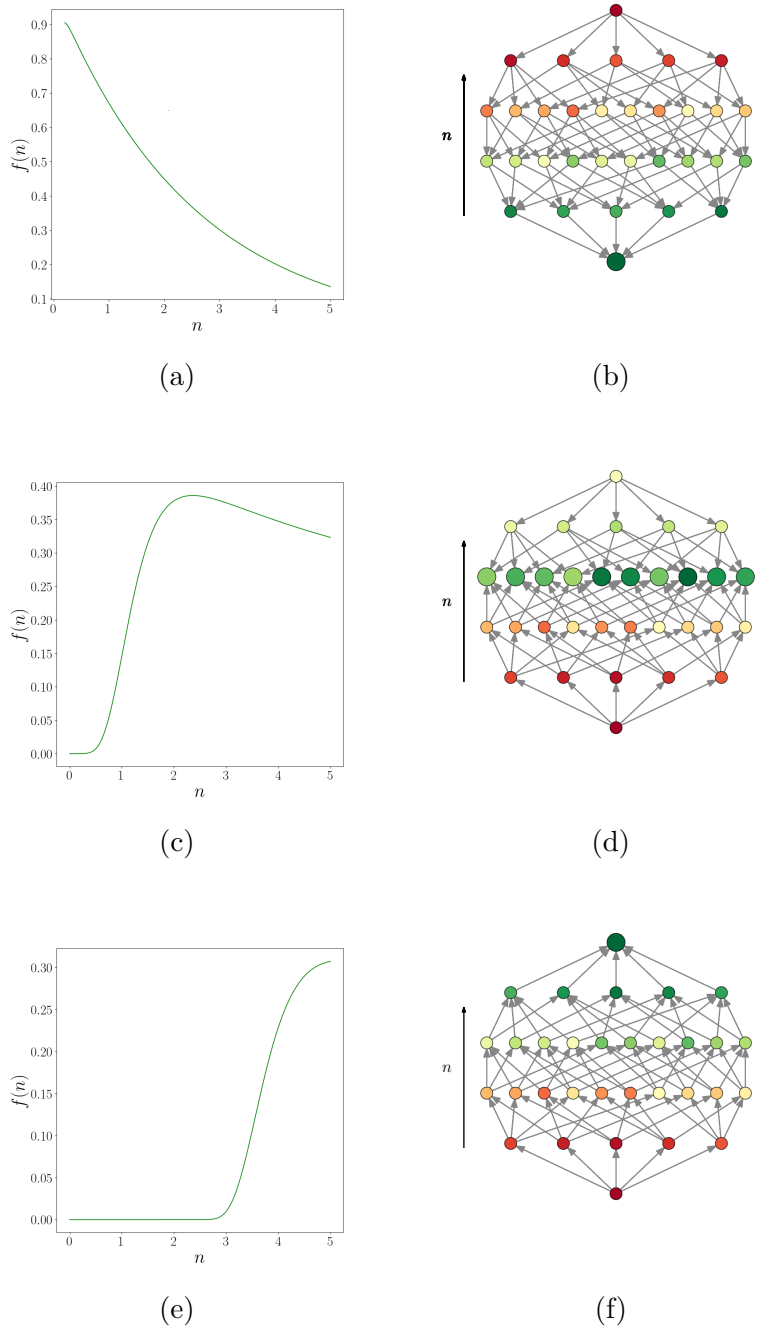

Figure 19: Fitness function shapes of TIL accessibility. (a), (c) and (e) are the fitness function shapes which conserve TIL accessibility property namely decreasing, concave and increasing functions. (b), (d) and (f) are respective deterministic fitness landscapes displaying the TIL accessibility property.

$$\frac{d(\ln(f(n))}{dn} = \frac{\alpha\nu(nv)^{\nu}}{n(1+e^{\alpha((nv)^{\nu}-\chi)})} - \frac{\mu(un)^{\mu}}{n}, \tag{33}$$

which indicates two shapes of the function $f(n)$ as n is varied. In the case χ is small enough, the derivative is negative and $f(n)$ always decreases. In this case, the wild type is the only peak. In the other case, χ is large enough so that the derivative starts positive but eventually becomes negative as n increases. This represents the concave case where a layer beyond $n = 0$ hosts the peaks while being accessible from the other layers. The derivative suggests a perfectly TIL accessible picture however, this analysis has a blind spot, that is, the derivative being undefined around the wild type ($n = 0$).

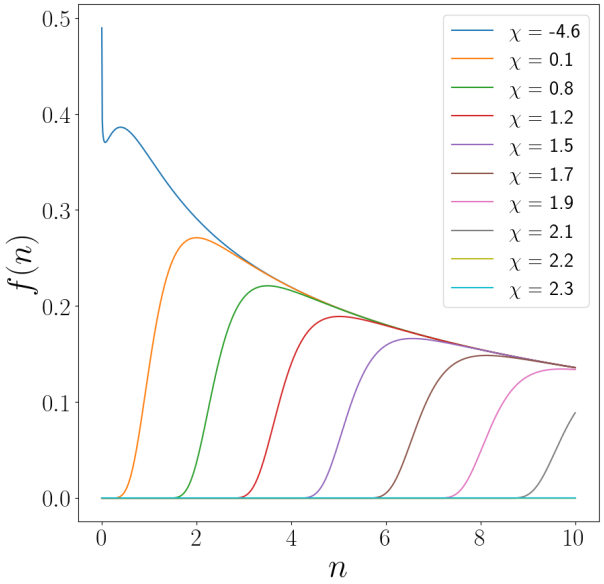

Figure 20: As χ changes, the shape of the fitness function changes. At low concentration, the fitness function hosts two layers of fitness peaks, indicating a persistent genotype. The system featured is for parameters ($u = v = 1, \mu = 0.3, \nu = 0.9$).

The TIL accessibility property will be broken if the wild type fitness $f(0)$ is greater than the fitness of the first mutants $f(1)$ for a concentration χ that is sufficiently large where $f(n)$ is concave; a scenario satisfied with the following inequalities:

$$\ln(f(0)) > \ln(f(1)) \ , \ \frac{df(n)}{dn} > 0. \tag{34}$$

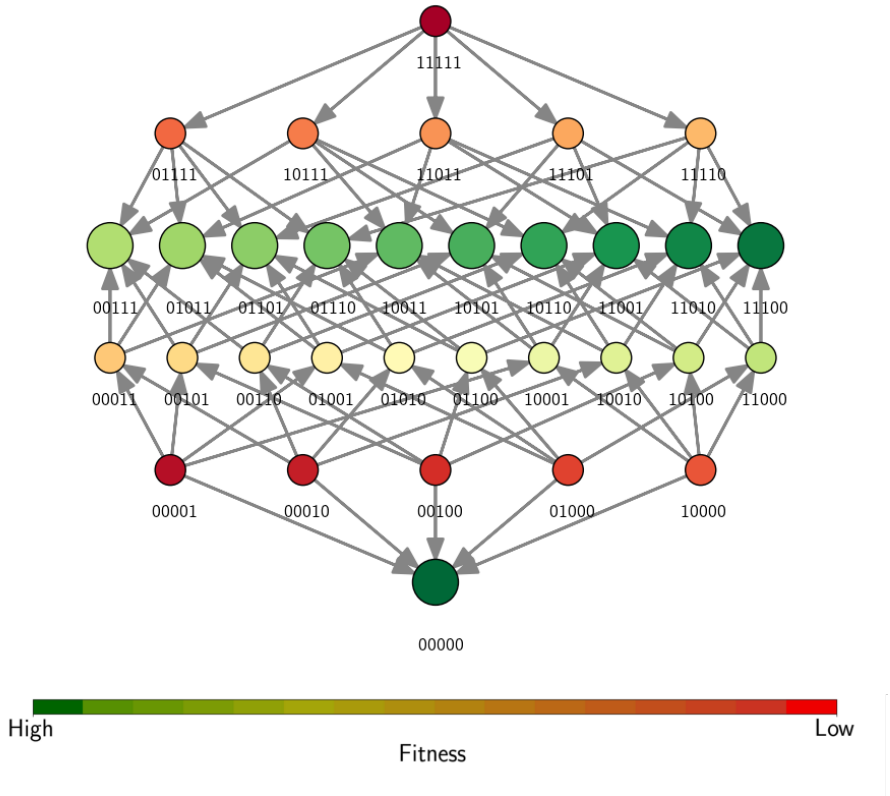

Figure 21: Diminishing returns epistasis breaks TIL accessibility by featuring another layer of peaks alongside a persistent wild type, making the second peak inaccessible from the wild type.

The regime of parameters satisfying these inequalities allows for the wild type to persist as a peak while another layer of peaks is propagating through the higher layers of the landscape. Such a regime will be referred to as the regime of a *persistent wild type* (Fig. 20 and 21). Persistence occurs for low values of IC_{50}, conditioned by $\mu < \nu$. The lower the value of v the larger the concentration range of persistence. The larger the concentration range, the more robust is the persistence upon introducing stochasticity in u and v. The persistence of the wild type could be justified by the fact that diminishing returns epistasis speeds up the loss of advantage of mutants with low number of mutations, creating peaks of their super-sets. This happens before the wild type loses its advantage, leading to the split of the landscape into two parts of evolution bias.

The result above is found at the continuous limit of the fitness function ($\lim_{n\to\infty} f(n)$). Since a landscape is a discrete fitness function of n, we expect the accessibility breaking to occur at the wild type but with a varying basin of attraction. The basin of attraction is, in this context, the number of layers whose adaptive walk is directed towards the wild type.

In a landscape with a second layer of fitness peaks, the number of layers n in the basin of attraction of the wild type can be found by minimizing the discrete fitness function, $f(n-1) > f(n)$ and $f(n) < f(n+1)$,

$$\frac{\ln\left(\frac{1+e^{\alpha(\chi-((n-1)v)^{\nu})}}{1+e^{\alpha(\chi-((n)v)^{\nu})}}\right)}{n^{\mu}-(n-1)^{\mu}} < u^{\mu} < \frac{\ln\left(\frac{1+e^{\alpha(\chi-((n)v)^{\nu})}}{1+e^{\alpha(\chi-((n+1)v)^{\nu})}}\right)}{(n+1)^{\mu}-(n)^{\mu}} \tag{35}$$

where the LHS is an increasing function in n while the RHS is a decreasing function in n. This makes TIL accessibility breaking by a basin of attraction more likely to be confined within layers with a low number of mutations n.

A result that is interesting to feature is the fact that as χ goes to infinity, there is a regime of parameters for which the fitness function is strictly convex with two peaks at the wild type and the full mutant, where

$$0 < \mu = \frac{\ln(\alpha v^{\nu})}{\ln(u)} < 1. \tag{36}$$

In most cases, the adaptation walks remain largely skewed towards the full mutant.

4.4 Fitness Epistasis in the TILME model

In the special case of deterministic TILME model discussed above, the TIL accessibility was found to hold beyond the wild type. A more general conclusion about TIL accessibility in the TILME model can be derived from the epistasis trend in fitness. Given the fitness function definition in eq. (22), the epistasis in fitness is given by:

$$\begin{aligned}\epsilon(f_{\boldsymbol{\sigma}}) = &-\Big(\sum_{i\in I^{+}} u_i\Big)^{\mu} - \ln\big(1+\big(e^{\alpha(\chi-(\sum_{i\in I^{+}} v_i)^{\nu})}\big)\big) \\ &+ \sum_{i\in I^{+}} (u_i)^{\mu} + \sum_{i\in I^{+}} \ln\big(1+\big(e^{\alpha(\chi-(v_i)^{\nu})}\big)\big)\end{aligned} \tag{37}$$

which is always positive for $\mu < 1$. This is a *Universal Positive Epistasis* picture which allows for forbidden orders to arise violating TIL accessibility. This theoretical result matches the experimental outcome in Figure 13. Approaching a rigorous description of the landscape dynamics in the the stochastic TILME landscapes, a semi-deterministic landscape is discussed next.

5 Semi-Deterministic Model of Magnitude Epistasis

After introducing magnitude epistasis to a deterministic version of the TIL model, in this chapter, a more realistic picture is approached by assuming stochasticity in the null-fitness inspired by the quantized TIL model (Q-TIL). In the Q-TIL model, each mutation contributes a constant advantage to the resistance, making the genotypes carry quantized values of resistance. The Q-TIL model was initially conceived in notes by Suman Garaub Das, Joachim Krug, and Muhittin Mungan to investigate the dynamics of adaptive walks on fitness landscapes. In this chapter, the Q-TIL model is approached from the perspective of the ordering rules of the IPs. In Subsection 5.1.1, results already found by Das et al. are presented along with the interesting features of the strong path and the long-lived peaks. After understanding the evolution dynamics of what will be referred to as the Q-TIL class of landscapes, diminishing returns epistasis adds a few layers of complexity to the landscape dynamics, which is studied in Section 5.2.

5.1 Q-TIL Class Landscapes

In the Q-TIL model, it is assumed that all mutations contribute to the IC_{50} equally

$$v_i = v, \qquad v_{\boldsymbol{\sigma}} = nv, \tag{38}$$

where n is the size of the set of mutations I^+. The IPs between the wild type $\mathbf{0}$ and the single mutants $\mathbf{0}^{+j}$ are defined as

$$\chi^*_{\mathbf{0},+j} = \ln\left(\frac{1-e^{-u_j}}{e^{-u_j}-e^{-\alpha v}}\right)^{\frac{1}{\alpha}}. \tag{39}$$

In the regime of interest (where $u_j, v > 0$), these IPs carry the same order as the null-fitness vector in eq. (19),

$$\chi^*_{\mathbf{0},+1} < \chi^*_{\mathbf{0},+2} < \cdots < \chi^*_{\mathbf{0},+L}. \tag{40}$$

As n increases, the IPs between genotypes with n mutations and genotypes with $n+1$ mutations will always hold the same order, but with a shift of size nv compared to the IPs values of the wild type (Fig. 22),

$$\chi^*_{\boldsymbol{\sigma},+j} = nv + \ln\left(\frac{1-e^{-u_j}}{e^{-u_j}-e^{-\alpha v}}\right)^{\frac{1}{\alpha}}. \tag{41}$$

IPs are only dependent on n and the proxy of the cost of the mutation j, u_j. The identity of the background $\boldsymbol{\sigma}$ is irrelevant but merely the number of the mutations a genotype carries. Hence, $\boldsymbol{\sigma}$ is simply indicated here by $\boldsymbol{n}$. Practically speaking, due to quantizing $v_{\boldsymbol{\sigma}}$, all IPs between genotypes of the same background size and a genotype differing by a single mutation j occur at the same concentration $\chi^*_{\boldsymbol{n},j}$.

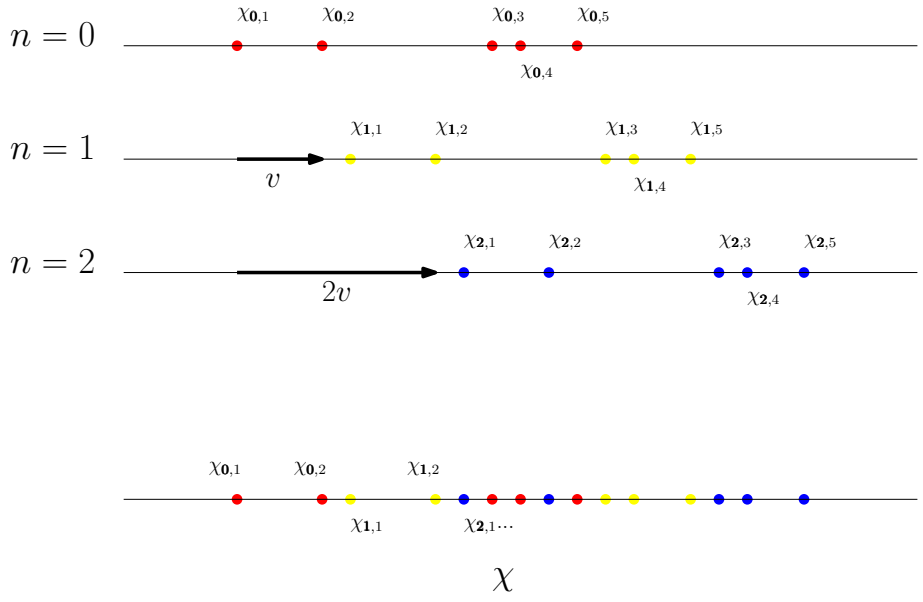

Figure 22: In the Q-TIL model, IPs ($\chi_{\boldsymbol{n},+j}$) have the same order in each layer n shifted to higher concentrations by nv. IPs from the same layer were given a distinct color.

Eq (41) implies the following ordering rules,

$$\chi^*_{\boldsymbol{n},+j} > \chi^*_{\boldsymbol{n-1},+j} \tag{42}$$

and

$$\chi^*_{\boldsymbol{n},+j} > \chi^*_{\boldsymbol{n},+(j-1)}. \tag{43}$$

The first rule is a special case of eq. (14). Therefore, the TIL accessibility applies in this case as well. These two inequalities are the defining rules of the *Q-TIL class landscapes*, and help reveal the dynamics of evolution on such a landscape.

5.1.1 Long-lived Peaks and the Strong Path

To picture the dynamics on a Q-TIL landscape, one keeps in mind the requirement for a genotype $\boldsymbol{\sigma}$ to be a fitness peak at a concentration χ,

$$\max_i(\chi^*_{\boldsymbol{n},-i}) < \chi < \min_j(\chi^*_{\boldsymbol{n},+j}) \tag{44}$$

or namely, χs have to be between all mutation-decreasing IPs and all mutation-increasing IPs relative to a genotype $\boldsymbol{\sigma}$ (Fig. 23). Mutation-decreasing IPs ($\chi^*_{\boldsymbol{n},-i}$) are defined as the ones reporting the intersection events between the dose-response curves of a genotype ($\boldsymbol{\sigma}$) with n mutations ($|I^+| = n$) and genotypes of size $n-1$ lacking the mutation i, while mutation-increasing IPs ($\chi^*_{\boldsymbol{n},+j}$) will indicate intersections between a genotype $\boldsymbol{\sigma}$ and genotypes of size $n+1$ having an additional mutation j.

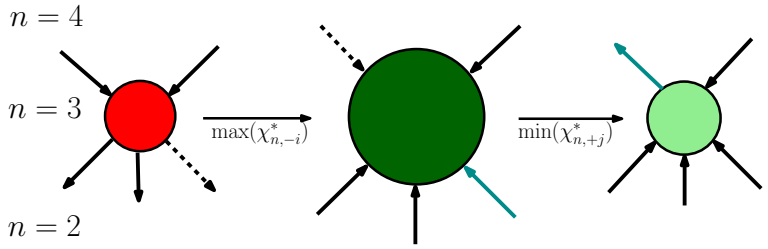

Figure 23: Conditions for gaining and losing peakness. (a) Concentration doses below the minimum required for mutation-decreasing edges (dashed) to flip. (b) All mutation-decreasing edges (blue) flipped, creating a fitness peak. (c) The minimum mutation-increasing edge (blue) flipped with which the node loses its peakness.

Now we define key terms in the Q-TIL class dynamics. We start with **peaks intervals**, or intervals of concentration where peaks carry a specific mutations number. In such an interval, a **long-lived peak** refers to a fitness peak that emerges the first and loses peakness the last. In this context, a **strong evolution path** is the greedy walk path or the path maximizing fitness in each step from the wild type to the full mutant on a landscape.

In the following we claim that:

- Fitness peaks emerge in disjoint *peaks intervals* of a unique number of mutations. These intervals, while disjoint, cover the whole concentration axis. This result was already observed in the notes of Das et al.

- In each of these intervals, a *long-lived peak* dominates the interval being also the fittest among all peaks.

- There exists a direct path between the *long-lived peaks* of all intervals, creating a *strong evolution path* to the full mutant.

In order to build up arguments for the above stated claims we start by asking the following question: In an increasing concentration scheme and in a layer of genotypes with n mutations, which genotype obtains peakness the first? This genotype must have all the mutation-decreasing edges flipped in its direction the earliest. Consequently, the associated set of mutations I^+, corresponds to the set of n smallest IPs.

Now to complete the picture, we ask the opposite question: Which genotype loses its peakness the latest? For a fitness peak to lose peakness, it takes one of the mutation-increasing edges to flip, pointing away. In other words, we are looking for the complement set I^- of size $L-n$ whose smallest element j maps to the largest $\chi^*_{\boldsymbol{n},+j}$. The search for the smallest I^+, and I^- with the largest minimum j, leads to a single genotype which we call for the above mentioned properties the *long-lived peak* ($\boldsymbol{\sigma}_l$).

Keeping eq. (43) in mind, we look at subsets of size n of a finite set of size L. The subset carrying the smallest possible maximum element, has always its complement of size $L-n$ with the largest possible minimum among all complements. Namely, among all the subsets and their complements,

$$I^+ \in \boldsymbol{S}_n, \quad \boldsymbol{S}_n = \{I^+ : |I^+| = n\}, \tag{45}$$

$$I^- \in \boldsymbol{S}_{L-n}, \quad \boldsymbol{S}_{L-n} = \{I^- : |I^-| = L-n\}. \tag{46}$$

A long-lived peak is a genotype $\boldsymbol{\sigma}_l$ such that,

$$i_{l_{\max}} = \min_{I^+ \in \boldsymbol{S}_n} (\max_{i \in I^+}(i)) \tag{47}$$

and

$$j_{l_{\min}} = \max_{I^- \in \boldsymbol{S}_{L-n}} (\min_{j \in I^-}(j)) \tag{48}$$

where $I^-(\boldsymbol{\sigma}_l) \cap I^+(\boldsymbol{\sigma}_l) = \emptyset$. From now on, we will use the generalized symbol $\boldsymbol{\sigma}$ to refer to genotypes that are not long-lived peaks.

In order to build the set $I^+(\boldsymbol{\sigma_l})$ of n elements from the set $I = \{1, 2, .., L\}$, the smallest possible maximum must be n. The complement of this set has to start with $n + 1$. All other mutation sets $I^+(\boldsymbol{\sigma})$ of size n have to have at least one element $i > n$, and their complements $I^-(\boldsymbol{\sigma})$ must contain at least one element $j < n + 1$. Therefore, in a layer n

$$i_{l_{\max}} = n, \quad \text{and} \quad j_{l_{\min}} = n + 1, \tag{49}$$

where $I^+(\boldsymbol{\sigma}_l) = \{1, 2, .., n\}$ and $I^-(\boldsymbol{\sigma}_l) = \{n + 1, n + 2, .., L\}$, and

$$I^-(\boldsymbol{\sigma}_l) \cap I^+(\boldsymbol{\sigma}_l) = \emptyset. \tag{50}$$

Long-lived peaks dominate the layer they belong to, being the fittest peak and a fitness peak throughout the concentration interval through which mutants with n mutations are candidates for peakness, where for $\forall \quad \sigma \neq \sigma_l$ in a layer n

$$\max(I^+(\boldsymbol{\sigma}_l)) < \max(I^+(\boldsymbol{\sigma})), \quad \max(i) \in I^+(\boldsymbol{\sigma}) > n \tag{51}$$

. and

$$\min(I^-(\boldsymbol{\sigma}_l)) > \min(I^-(\boldsymbol{\sigma})), \quad \min(j) \in I^-(\boldsymbol{\sigma}) < n + 1. \tag{52}$$

The peaks interval in which genotypes with n mutions are candidates of being peaks has width $w(n)$ defined by $j_{l_{\min}}$ and $i_{l_{\max}}$,

$$w(n) = \chi^*_{\boldsymbol{n},+j_{l_{\min}}} - \chi^*_{\boldsymbol{n},-i_{l_{\max}}} \tag{53}$$

marking the difference between the concentrations at which the long-lived peaks emerge in layers $n + 1$ and n.

It is worthwhile to explicitly state that the genotype $\boldsymbol{\sigma}_l$ losing peakness in layer n is the sign of the emergence of the long-lived peak in the layer $n + 1$,

$$\max_{I^+ \in \boldsymbol{S}_{n+1}} (i) = \min_{I^- \in \boldsymbol{S}_{L-n}} (j). \tag{54}$$

Furthermore, eq. (54) implies that these intervals of long-lived peak, while disjoint, are covering the entire concentration axis.

It follows from eq. (54) and the structure of $\boldsymbol{\sigma}_l$, that the long-lived peaks are easily identified and connected by a direct path. At $n = 1$, the long-lived peak has the mutation set $I^+(\boldsymbol{\sigma}_l) = \{1\}$, at $n = 2$, the mutation set is

$I^+(\boldsymbol{\sigma}_l) = \{1, 2\}$, at $n = a$, the mutation set is $I^+(\boldsymbol{\sigma}_l) = \{1, 2, .., a\}$, and so on up to $n = L$. This direct path of connected long-lived peaks will be the unique path for evolution from the wild type to the full mutant under a quasi-static concentration protocol. This path will be referred to as the *strong path*.

5.1.2 Ruggedness of the Q-TIL Landscapes

Due to the fact that increasing-mutation edges will start flipping away before *all* decreasing-mutation edges flip, pointing towards $\boldsymbol{\sigma}$, genotypes with $\max(\chi^*_{\boldsymbol{\sigma},-i}) > \chi^*_{\boldsymbol{\sigma},+j_{l_{\max}}}$ will never become peaks.

The opposite case, with all $\chi^*_{\boldsymbol{\sigma},-i} < \chi^*_{\boldsymbol{\sigma},+j_{l_{\min}}}$, indicates the case of maximum ruggedness with each layer having a window of concentration for which all genotypes are peaks. Minimum ruggedness can also be directly inferred from maximizing the overlap between IPs from different layers

$$\chi^*_{\boldsymbol{n},-n} < \chi^*_{\boldsymbol{n},+n} < \chi^*_{\boldsymbol{n},-(n+1)} < \chi^*_{\boldsymbol{n},+(n+1)}, \tag{55}$$

where this arrangement allows only for the rise of a single peak. The IP marking the transition of the long-lived peak $\chi^*_{\boldsymbol{n},+(n+1)}$ (from layers n to $n+1$) always appears after $\chi^*_{\boldsymbol{n},-(n+1)}$. It is clear that while $\chi^*_{\boldsymbol{n},-(n+1)}$ could potentially give rise to additional peaks, the arrangement in eq. (55) ensures that one mutation-increasing edge for these potential peaks has already flipped allowing no peaks alongside $\boldsymbol{\sigma}_l$.

Ruggedness depends on the spread of the IPs. If the spread of the IPs in a layer n covers a range less than v, the shift unit, the landscape achieves maximum ruggedness. If the spread is greater than v, the overlap of the IPs from different layers increases with the number of mutations n. Landscapes can be thought of as a symmetric configuration of genotypes with respect to the central layer, where the structure below the central layer is a mirror image of the structure above. When v is constant, the number of peaks in both structures is the same. For a shrinking v, the number of peaks in the upper half can be less than in the lower half as the peaks intervals shrink with increasing n.

Now we motivate the largest number of fitness peaks in the interval n at arbitrary concentration. It can be found through identifying the mutation related to the largest mutation-decreasing IP less than $\chi^*_{\boldsymbol{n},+j_{l_{min}}}$, we call the index of this mutation K defined as

$$K = \underset{i}{\text{argmax}}(\chi^*_{\boldsymbol{n},-i}) < \chi^*_{\boldsymbol{n},+j_{l_{min}}}. \tag{56}$$

In order to take care of potential overlap between the intervals spanning mutation-increasing IPs and mutation-decreasing IPs, we define the largest mutation index related to mutation-increasing IPs less than $\chi^*_{\boldsymbol{n},-K}$, labeled as k. The index k is given by

$$k = \underset{j}{\text{argmax}}(\chi^*_{\boldsymbol{n},+j}) < \chi^*_{\boldsymbol{n},-K}. \tag{57}$$

The maximum number of fitness peaks in the nth peak interval is then given by the following binomial,

$$M(n) = \binom{K-k}{n-k} \geq 1. \tag{58}$$

Note that this binomial counts all possible sequences $\boldsymbol{\sigma}$ made up of n mutations, which satisfy the relation in eq. (44). At a concentration χ, defining the number of fitness peaks one has to find n for which

$$\chi^*_{\boldsymbol{n},+n} < \chi < \chi^*_{\boldsymbol{n+1},+(n+1)}. \tag{59}$$

Identifying n, now one has to adjust the right-hand sides of the inequalities in (56) and (57) to χ. We will call the values resulting from this adjustment $\tilde{K}$ and $\tilde{k}$ respectively. The number of peaks in such a landscape is

$$m(\chi) = \binom{\tilde{K}-\tilde{k}}{n-\tilde{k}}. \tag{60}$$

Notice that all results in section (5.1) follow from inequalities (42) and (43). Any model satisfying these inequalities will have the properties described above. All such models fall into the *Q-TIL class*.

Now that we understand how a simple landscape with additive parameters and a constant IC_{50} behaves, it is time to introduce magnitude epistasis.

5.2 Magnitude Epistasis in Q-TIL Landscapes (Q-TILME)

Adding magnitude epistasis to the Q-TIL model (Q-TILME), we follow the scheme in section (4.1):

$$u_{\boldsymbol{\sigma}} = (\sum_{i \in I^+} u_i)^{\mu}, \; v_{\boldsymbol{\sigma}} = (nv)^{\nu} \tag{61}$$

where diminishing returns epistasis is attained for $0 < \mu < 1$ and $0 < \nu < 1$.

Our key formulas for fitness and IPs will be given by;

$$f_{\boldsymbol{\sigma}}(x) = \frac{e^{-(\sum_i^n u_i)^\mu}}{1 + \left(e^{\chi - (nv)^\nu}\right)^\alpha} \tag{62}$$

and

$$\chi^*_{\boldsymbol{\sigma},+j} = (nv)^\nu + \frac{1}{\alpha} \ln \left(\frac{1 - e^{-((\sum_i^n u_i + u_j)^\mu - (\sum_i^n u_i)^\mu)}}{e^{-((\sum_i^n u_i + u_j)^\mu - (\sum_i^n u_i)^\mu)} - e^{-\alpha(((n+1)v)^\nu - (nv)^\nu)}} \right), \tag{63}$$

where $j \in I^-$ and $i \in I^+$.

IPs here are constructed out of two parts, one is the shift part $(nv)^\nu$. The shift part reduces with n. The second part resembles the wild type IPs function in eq. (39), except it depends on the difference $((\sum_i^n u_i + u_j)^\mu - (\sum_i^n u_i)^\mu)$. Let's call this part $\widetilde{\chi^*_{\boldsymbol{n},+j}}$, a fictional IP which will be both dependent on u_j and the background $u_{\boldsymbol{\sigma}}$.

5.2.1 Background Independent Q-TILME Landscapes

Here, the IP's background dependence is assumed to be negligible. The effect of a shift of a changing size in the IPs in each layer is the way magnitude epistasis will introduce deviations from the simple Q-TIL model.

Note that $\chi^*_{\boldsymbol{0},+j}$, in the context of magnitude epistasis, are ordered like in the Q-TIL case,

$$\chi^*_{\boldsymbol{0},+j} = \frac{1}{\alpha} \ln \left(\frac{1 - e^{-(u_j)^\mu}}{e^{-(u_j)^\mu} - e^{-\alpha(v)^\nu}} \right). \tag{64}$$

In addition, weak background dependence in each layer n will guarantee that $\widetilde{\chi^*_{\boldsymbol{n},+j}}$ will follow the same order as $\chi^*_{\boldsymbol{0},+j}$. This picture is Q-TIL with a shrinking positive shift of IPs as n increases, which still satisfies the Q-TIL class inequalities in (42) and (43). As a consequence, such a landscape will have long-lived peaks and a strong path. Another consequence is peaks intervals which are exclusive for peaks with a unique mutation number n. The only difference between this case and the Q-TIL will be the width of the interval, where for the Q-TIL the width is greater than v,

$$w(n) = \chi^*_{\boldsymbol{n+1},+j_{l_{min}}} - \chi^*_{\boldsymbol{n},+i_{l_{max}}} = v + \chi^*_{\boldsymbol{0},n+1} - \chi^*_{\boldsymbol{0},n} \tag{65}$$

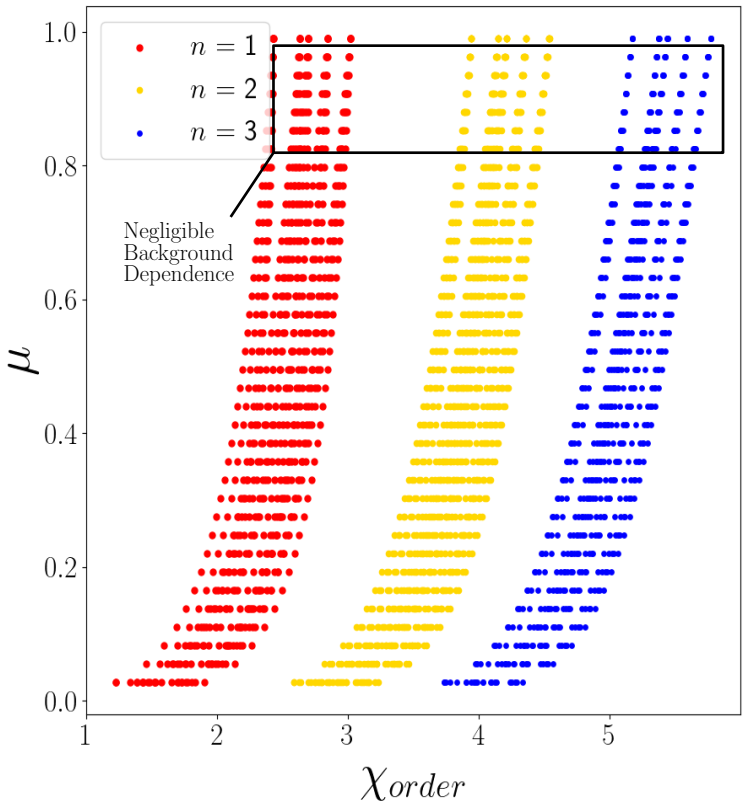

Figure 24: The configurations of IPs for different epistasis levels in the cost of mutations. Background dependence plays a role at high level of magnitude epistasis (low values of μ) where the dispersion of IPs is more pronounced. The IPs in this graph are for $\nu = 0.7$, $v = 6$ and $\overline{u} = 0.3$. Each layer n has a distinct color.

whereas the width in the Q-TILME case with weak background dependence can be less than v,

$$\widetilde{w}(n) = \chi^*_{\boldsymbol{\sigma},+j_{l_{min}}} - \chi^*_{\boldsymbol{\sigma},-i_{l_{max}}} = ((n+1)^\nu - n^\nu)v^\nu + \widetilde{\chi^*_{\mathbf{0},n+1}} - \widetilde{\chi^*_{\mathbf{0},n}}. \tag{66}$$

Landscapes here are expected to have a lower ruggedness than the epistasis-free case as the shrinking shift in the IPs order brings a higher chance of overlap of IPs from different layers, especially at high n. At low epistasis levels, a Q-TILME with weak background dependence is expected (Fig. 24).

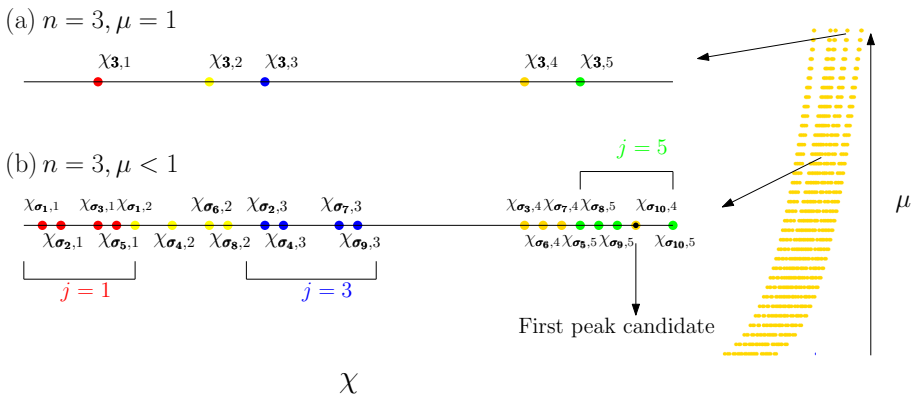

Figure 25: The background dependence makes each IP unique creating a dispersion effect from a point to a cluster of $\binom{L-1}{n}$ points. (a) Q-TIL order of n points. (b) Q-TILME order of $\left(\binom{L-1}{n}L\right)$ points. Notice that each cluster is given a distinct color here.

5.2.2 Background Dependent Q-TILME

In order to study diminishing returns epistasis with strong background dependence in the context of Q-TILME model, the changes in the configuration of the IPs are first introduced. The following arguments focus on mutation-increasing IPs describing dose-response curves intersections between any two neighboring genotypes. One of these two genotypes acquired an additional mutation j on top of the mutation set of the other genotype $\boldsymbol{\sigma}$. This latter genotype will be referred to as the background genotype. The $(+)$ sign in mutation increasing IPs $(\chi^*_{\boldsymbol{\sigma},j})$ is dropped for simplicity.

In the absence of epistasis, the identity of the background $\boldsymbol{\sigma}$ to which a mutation is added was irrelevant in defining IPs. IPs between a genotype $(\boldsymbol{\sigma})$ and a genotype differing by a single mutation j $(\boldsymbol{\sigma}^{+j})$ occur at an order solely dependent on the identity of the mutation j. In Figure 25 (a), multiple IPs overlap projecting $\left(\binom{L-1}{n}L\right)$ IPs on L points for no or weak epistasis levels.

In Figure 25 (b), the background dependence recovers the full $\left(\binom{L-1}{n}L\right)$ IPs, as the contribution from the background sum $(\sum_i^n u_i)$ results in a unique point for each pair of genotypes. The background effect will be referred to as the *dispersion* of IPs. Notice that this dispersion effect is centered around the values where IPs overlap in the absence of epistasis. This dispersion effect is proportional to the epistasis level. Stronger the epistasis, further apart are the IPs related to a particular mutation j. The resulting picture is IPs of

different backgrounds clustering together in groups. These clusters are ordered depending on the u_j. The effect of these clusters overlapping on the landscape dynamics will be one source of deviation from the Q-TIL picture.

5.2.3 The Impact of Cluster Overlap

The dispersion of the IPs lead to the rise of clusters of points, whose chance of overlapping increases with the increase in epistasis levels, both in the cost of mutations and the resistance they bring (Fig. 24 and 27). Assuming IPs from different layers do not overlap, the main source of deviation from the Q-TIL class dynamics here will be overlap of clusters. The clusters will also be labelled by the identity of the added mutation defining the IPs, namely j.

In each cluster j, the IPs are ordered depending on the background, where $\chi_{\boldsymbol{\sigma},j}$ is a decreasing function of the sum $(\sum_i^n u_i)$. These background genotypes defining the order of the IPs in each cluster will be labelled $\boldsymbol{\sigma_k}$, where $\boldsymbol{\sigma_1}$ is the genotype of the largest sum $(\sum_i^n u_i)$ and $\boldsymbol{\sigma_N}$ is the genotype of the minimum sum in the cluster, where $N = \binom{L}{n}$.

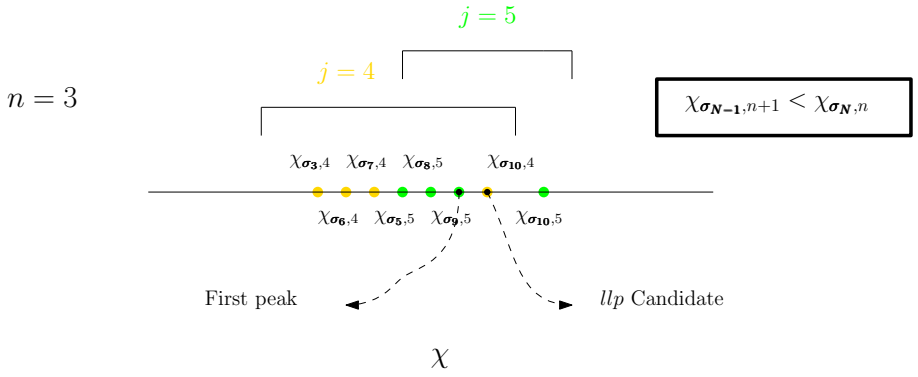

Figure 26: The overlap of two clusters, where cluster 4 is given in yellow and cluster 5 is given in green. the first peak emerges after $\chi_{\boldsymbol{\sigma}_9,5}$ before the emergence of the long-lived peak (*llp*) at $\chi_{\boldsymbol{\sigma}_{10},4}$. Overlap of clusters can cause peaks intervals overlap, leading to the emergence of peaks from different layers at the same concentration.

Now we have a picture of L clusters of IPs ordered directly with respect to u_j. In each of these clusters there are $\binom{L-1}{n}$ points ordered following the background sum. Looking into the key landscape dynamics, we know that the long-lived peak candidate has to be the one with the mutation set $I^+ =$

$(1, 2, .., n)$. This candidate becomes a peak between the IPs $\chi_{\boldsymbol{\sigma_N},n}$ and $\chi_{\boldsymbol{\sigma_N},n+1}$. Due to the direct dependence on u_j, it is the case in the layer $n+1$ that

$$\chi_{\boldsymbol{\sigma_k},j} < \chi_{\boldsymbol{\sigma_N},n+1} \tag{67}$$

for all $j \leq n+1$, making this candidate the peak that loses peakness the last.

However, it is not guaranteed that this candidate will be the first to become a peak, since in layer n for $j > n$, and due to the inverse dependence on the sum $(\sum_i^n u_i)$, the inequality $\chi_{\boldsymbol{\sigma_k},j} < \chi_{\boldsymbol{\sigma_N},n}$ can be true. Notice here that if $\chi_{\boldsymbol{\sigma_N},n}$ is preceded by $\chi_{\boldsymbol{\sigma_{N-1}},n+1}$ in layer n, another peak will emerge before the long-lived peak transition occurs in layer n, creating an overlap between peaks intervals. Peaks from different layers can now occur at the same concentration, and the notion of a long-lived peak is irrelevant (Fig. 26).

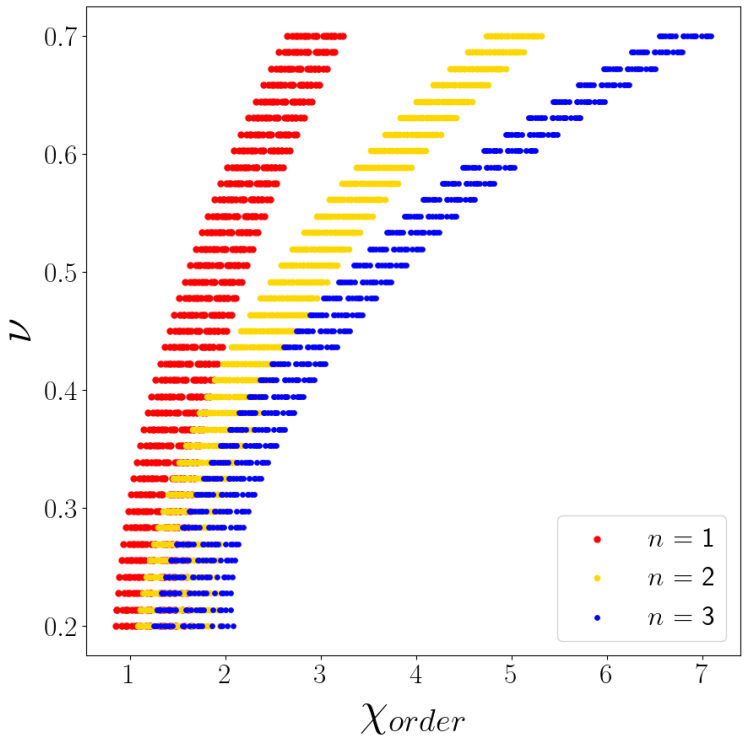

Figure 27: The configurations of IPs for different epistasis levels in the IC_{50}. The overlap of layers plays a role at high level of magnitude epistasis (low values of ν) where the shifts are insufficient to create separate regimes for IPs from different layers. The IPs in this graph are for $\mu = 0.4$, $v = 6$, and $\overline{u} = 0.3$.

On the other hand, the strong path will survive the clusters overlap as the genotypes forming the strong path will always be the fittest in their layers

and the last to transition to the next layer. Since we are not considering layers overlap, the TIL accessibility will still hold. As for the ruggedness, the dispersion level controls the spread of IPs. Higher the dispersion the less likely a genotype will fulfill peakness conditions.

These results assume no layers overlap. The overlap of layers occur at higher levels of magnitude epistasis, especially in the IC_{50} (Fig. 27). The strong path property will only fail if the overlap of IPs from different layers is strong enough such that the IP candidate to create a long-lived peak ($\chi_{\boldsymbol{\sigma_N},n}$) from a higher layer precedes the one from a lower layer. As a consequence, some peaks intervals could vanish since some layers may carry no peaks. In this scenario, the TIL accessibility will be violated and ruggedness is expected to be low.

6 Discussion and Outlook

In Chapter 3, the assumptions of the TIL model, being a parameterized fitness function with interesting properties, were tested in the context of experimental data of β-lactam resistance. This discussion starts by outlining the deviations found in the experimental results compared to the theory in an attempt to map developments on the model.

A remarkable observation was that the growth curves fell into different phases, one of which imposed a significant challenge in this analysis. The fluctuating phase compared to the stable phase in Figure 7 had irregular unsteady growth curves in each replicate around the MIC concentrations, where the population was stressed. This might be explained by the fact that in response to stress, *E. coli* filaments sometimes, enhancing tolerance through delayed cell division [23]. The elongated cells burst once the growing pressure cannot be held within the cell wall. This mechanism might justify the spike in the OD followed in few hours layer by a drop. It might also be the case that the replicates were not clonal leading to varying response paces, creating the divergent behavior among replicates.

In all cases, the logistic function describing the exponential growth of a population up to the environment capacity was not reflective of the observed growth curves. Therefore, the area under the curve (AUC) was preferred over a growth rate extracted from an exponential fit.

Being careful not to take into account apparent growth that might result from a cell response rather than a cell division, only few hours of initial exponential growth was considered. Even after the cutoff, one could notice that many genotypes experienced higher level of growth in the presence of stress compared to the stress free case, posing the need to investigate further the behavior of populations under pressure and to revise the basic model of the dose-response curves.

Having a stable measure of fitness now, the raw data was translated into tangible results by fitting the dose-response curves to the usual Hill function in eq. (12) (Fig. 9). While the data carried dose-response curves of pronounced epistasis that weakened tradeoff, the fitness mostly increased or remained relatively the same as the concentration of the antibiotic increased, compared to genotypes with a subset of mutations. This monotonic behavior allowed for

an abundance of accessible evolutionary paths to the full mutant, a general behavior expected in the context of the TIL model.

Epistatic interactions between mutations were a major observation that the TIL model neglects. Diminishing returns epistasis was dominant in the IC_{50}, where the resistance growth with mutations was weaker than multiplicative. However, fitness was actually amplified by the positive epistasis in the null-fitness at low concentrations. This boosts fitness at absent or weak pressure due to the low cost mutations bring. The effect of low mutation cost was illustrated in the irreversible evolution trajectory shown by the state transition graph in Figure 16 . Epistasis trend in fitness was found to be dominantly positive. Given that diminishing returns in the cost of mutations boosts fitness, this is not surprising. However, the shrinking of the IC_{50} didn't impact the acceleration in adaptivity, both in the experimental results (Fig 13) and the theoretical model proposed (eq. (37)).

The detailed results of this experiment should not be considered conclusive as the resolution of the data was low, where a cutoff needed to be introduced to the growth curves. Moreover, the gradient of concentrations used to produce these data was high, where out of 11 concentrations all genotypes were already dead in the last two. This shifts the range of experiment out of the informative regime. However, the dominant trends of magnitude epistasis both in the null-fitness and the IC_{50}, that laid the ground for dominant positive epistasis trend in fitness, are major deviations from the TIL model, that are interesting to theoretically investigate.

Chapter 4 was dedicated to introducing magnitude epistasis to the framework of the TIL model. Applying a diminishing returns TIL fitness function, the mathematical parameters indicating the level of epistasis in the cost of mutations (μ) and the IC_{50} (ν) were then extracted from the experimental data. Diminishing returns epistasis was stronger in the cost of mutations compared to the IC_{50} in the experiment analyzed here.

Moving away from the experimental constraints, the impact of magnitude epistasis on the highly rugged, highly accessible TIL landscapes was investigated. In the deterministic limit of the model, it was found that landscapes characterized with low resistance advantage and levels of diminishing returns in the cost higher than those in the resistance, the wild type could persist. This means creating a landscape with two basins of attraction where it is unlikely

to reach the fittest layer of genotypes from the wild type. In the experimental results shown in Chapter 3, the landscapes in the absence and at low levels of stress displayed a similar feature. Due to the absent cost of mutations, a second peak emerged along with the wild type and the single mutants peaks.

Approaching a more realistic picture, diminishing returns epistasis in semi-deterministic landscapes was studied in chapter 5. Semi-deterministic landscapes that are epistasis free hold characteristic dynamics along with trivially guaranteeing the TIL-accessibility. Employing the ordering rules of the IPs, one can define general properties of the dynamics of evolution on a resistance quantized landscape (Q-TIL). Intervals of peaks of unique number of mutations dominated by long-live peaks are two features that enable the emergence of a strong path of evolution in which the greedy evolutionary trajectory from the wild type to the full mutant on a landscape is explicitly known. Introducing epistasis of the diminishing returns nature, the Q-TIL properties show dependence on the level of epistasis. For weak levels of epistasis, all the properties mentioned above continue to hold.

Increasing epistasis levels reveals two different regimes. The first regime is when the clusters structure of the IPs in a given layer n starts to overlap. This endangers the properties of peaks intervals along with the long-lived peaks, however the strong path along with the TIL-accessibility are still guaranteed. The second regime is at higher epistasis levels that derive IPs from different layers to overlap, all the above mentioned properties including the TIL-accessibility, are compromised. This later case points out that the gradual growth in the number of mutations for the peaks as the pressure is increased is not the case whenever epistasis is very high. The random arrangement of IPs makes it more likely that few genotypes will dominate the landscapes as the environment changes.

As for ruggedness, the IP's spread controls how many peaks a layer could develop. It was found that the spread of IPs depends on the epistasis parameters, indicating a decreasing ruggedness with increasing levels of epistasis compared to the epistasis free case. The main result in Chapter 5 was discovering the IPs ordering rules and their role in identifying systemic behavior in landscape dynamics along with revealing the accessibility and ruggedness nature of the landscapes.

For further studies, the data analyzed here suggests that the Hill functions

are an oversimplification of the dose-response behavior in bacteria. Rigorous experiments along with a better understanding of the response mechanisms of bacteria to pressure should help in formalizing more realistic models. Theoretically, it would be interesting to approach the ordering rules of the IPs and the underlying evolution dynamics from a fully stochastic picture, where the tradeoff parameters are sampled from pre-identified distributions. A better understanding of the nature of interactions between mutations, and the influential factors in this context like the size of the system or the environment, could enable the approach of more realistic models.

References

[1] O'Neill J. *Tackling drug-resistant infections globally: final report and recommendations*. Government of the United Kingdom, 2016, p. 11. URL: https://amr-review.org/sites/default/files/160518_Final%20paper_with%20cover.pdf.

[2] Murray J L et al. "Global burden of bacterial antimicrobial resistance in 2019: a systematic analysis". In: *The Lancet* 399 (2022), pp. 629–655. DOI: 0.1016/S0140-6736(21)02724-0.

[3] *Environmental Dimensions of Antimicrobial Resistance: Summary for Policymakers*. United Nations Environment Programme, 2022, p. 4. URL: https://www.unep.org/resources/report/summary-policymakers-environmental-dimensions-antimicrobial-resistance.

[4] Mwangi MM et al. "Tracking the in vivo evolution of multidrug resistance in Staphylococcus aureus by whole-genome sequencing." In: *Proceedings of the National Academy of Sciences* 104.22 (2007), pp. 9451–9456. DOI: 10.1073/pnas.0609839104.

[5] Wright S. "The roles of mutation, inbreeding, crossbreeding, and selection in evolution". In: 1 (Proc.Sixth. Int. Cong. Genet. 1932), pp. 356–366. URL: https://www.pe.ska.life.tsukuba.ac.jp/~toque/POPGEN/pdfs/Wright1932.pdf.

[6] de Visser J and Krug J. "Empirical fitness landscapes and the predictability of evolution". In: *Nature Reviews Genetics* 15 (2014). DOI: 10.1038/nrg3744.

[7] Bank C. "Epistasis and Adaptation on Fitness Landscapes". In: *Annual Review of Ecology, Evolution, and Systematics* 53.Volume 53, 2022 (2022), pp. 457–479. DOI: https://doi.org/10.1146/annurev-ecolsys-102320-112153.

[8] Das SG et al. "Predictable properties of fitness landscapes induced by adaptational tradeoffs". In: *eLife* 9 (May 2020). DOI: 10.7554/elife.55155.

[9] Couce A and Tenaillon OA. “The rule of declining adaptability in microbial evolution experiments”. In: *Frontiers in Genetics* 6 (2015). DOI: 10.3389/fgene.2015.00099.

[10] Schoustra S et al. “Diminishing-returns epistasis among random beneficial mutations in a multicellular fungus”. In: *Proceedings of the Royal Society B: Biological Sciences* 283.1837 (2016), p. 20161376. DOI: 10.1098/rspb.2016.1376.

[11] Das SG, Krug J, and Mungan M. “Driven Disordered Systems Approach to Biological Evolution in Changing Environments”. In: *Phys. Rev. X* 12 (3 Sept. 2022), p. 031040. DOI: 10.1103/PhysRevX.12.031040.

[12] Regoes RR et al. “Pharmacodynamic Functions: a Multiparameter Approach to the Design of Antibiotic Treatment Regimens”. In: *Antimicrobial Agents and Chemotherapy* 48.10 (2004), pp. 3670–3676. DOI: 10.1128/aac.48.10.3670-3676.2004.

[13] Gillespie JH. “Molecular Evolution Over the Mutational Landscape”. In: *Evolution* 38.5 (1984), pp. 1116–1129. DOI: 10.2307/2408444.

[14] Papkou A et al. “A rugged yet easily navigable fitness landscape”. In: *Science* 382.6673 (2023). DOI: 10.1126/science.adh3860.

[15] Krug J and Oros D. “Evolutionary accessibility of random and structured fitness landscapes”. In: *Journal of Statistical Mechanics: Theory and Experiment* 2024.3 (Mar. 2024), p. 034003. DOI: 10.1088/1742-5468/ad3197.

[16] King ES et al. “Fitness seascapes are necessary for realistic modeling of the evolutionary response to drug therapy”. In: *bioRxiv* (2022). DOI: 10.1101/2022.06.10.495696.

[17] Weinreich DM et al. “Darwinian Evolution Can Follow Only Very Few Mutational Paths to Fitter Proteins”. In: *Science* 312.5770 (2006), pp. 111–114. DOI: 10.1126/science.1123539.

[18] Zwietering MH et al. “Modeling of the Bacterial Growth Curve”. In: *Applied and Environmental Microbiology* 56.6 (1990), pp. 1875–1881. DOI: 10.1128/aem.56.6.1875-1881.1990.

[19] Marcusson LL, Frimodt-Møller N, and Hughes D. "Interplay in the Selection of Fluoroquinolone Resistance and Bacterial Fitness". In: *PLoS Pathog* 5.8 (2009). DOI: 10.1371/journal.ppat.1000541.

[20] Andersson DI and Hughes D. "Antibiotic resistance and its cost: is it possible to reverse resistance". In: *Nat Rev Microbiol.* 8(4) (2010), pp. 260–71. DOI: 10.1038/nrmicro2319.

[21] Wei X and Zhang J. "Patterns and Mechanisms of Diminishing Returns from Beneficial Mutations". In: *Molecular Biology and Evolution* 36.5 (Feb. 2019), pp. 1008–1021. DOI: 10.1093/molbev/msz035.

[22] Chou H et al. "Diminishing Returns Epistasis Among Beneficial Mutations Decelerates Adaptation". In: *Science* 332.6034 (2011), pp. 1190–1192. DOI: 10.1126/science.1203799.

[23] Kjeldsen TS, Sommer MO, and Olsen JE. "Extended spectrum β-lactamase-producing Escherichia coli forms filaments as an initial response to cefotaxime treatment". In: *BMC Microbiology* 15 (2015). DOI: 10.1186/s12866-015-0399-3.

[24] Kendall MG. *Rank Correlation Methods.* Springer US, 1981, pp. 146–163. DOI: 10.1007/978-1-4684-6683-6_9.

Supplementary Material

AUC Vs. Growth Rate (extended discussion)

This section is an extension of Subsection(3.2.2), here the growth rate and the AUC in the context of the given data as measures of fitness are compared to determine which is more appropriate to use and whether one corresponds to the other. The following discussion follows the order of the questions worked through to decide which measure of fitness to use.

The steady part of the growth considered in this analysis corresponds to the exponential phase of growth, so the extraction of the growth rate (R) from the four available data points was done by finding the maximum slope in the log scale between any two data points. The growth rate measure introduces a shape to the dose-response curves where a significant increase is observed prior to the decrease in fitness, which is poorly modeled by the Hill function (Fig. 28).

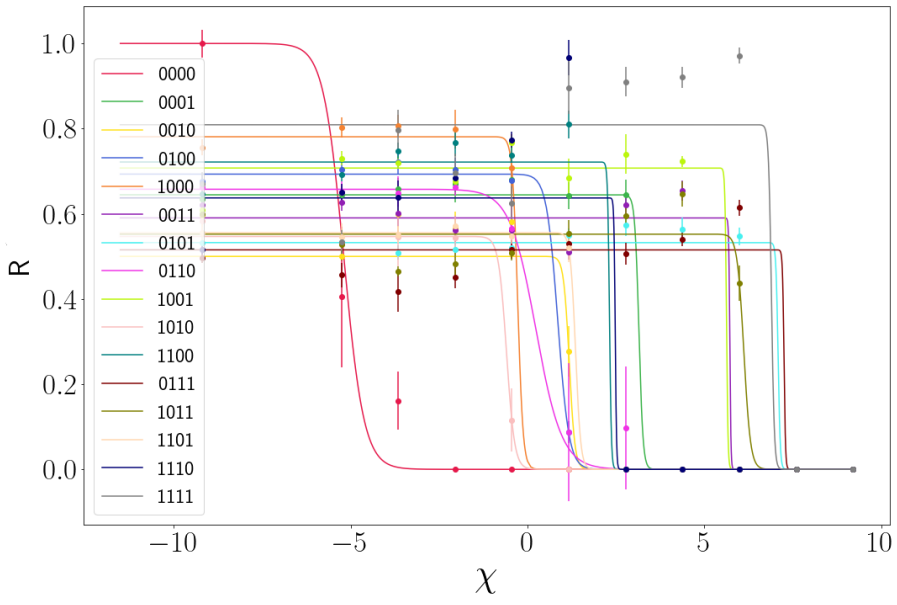

Figure 28: The dose-response curves taking the growth rate (R) in the steady part as a measure of fitness. The curves tend to have the highest fitness point at intermediate concentration. The Hill coefficient α was a fitted parameter here and took different values to enhance the fits. R is normalized with respect to the wild type's null-fitness and χ here is given in units of $\log(mg/ml)$.

The biomass defined by the area under the growth curve should be equivalent to the exponential growth rate in rank order, if all growth curves have the same behavior and are represented by the same logistic function. The area under the logistic curve (AUC) in eq. 18 was found:

$$AUC = (OD_{max} - OD_0)T + \frac{OD_{max}^2 \log(1 + \exp[\frac{4R}{OD_{max}}(t_{lag} - T) + 2])}{4R} + \frac{OD^2 \log(\exp[\frac{4R}{OD_{max}}(t_{lag}) + 2])}{4R} \quad (68)$$

where T is the total growth time of $5.5h$. The analytical AUC is a monotonically increasing function in R, which allows for the two measures to indicate fitness rank order interchangeably. In Figure (29), a range of $R = [0,2]$ in units of OD growth per hour (the range of the present experiment) has been plotted against the AUC for parameters of $OD_0 = 0.021$ and $OD_{max} = 0.5$, varying these parameters within the detected range doesn't change the monotonic trend.

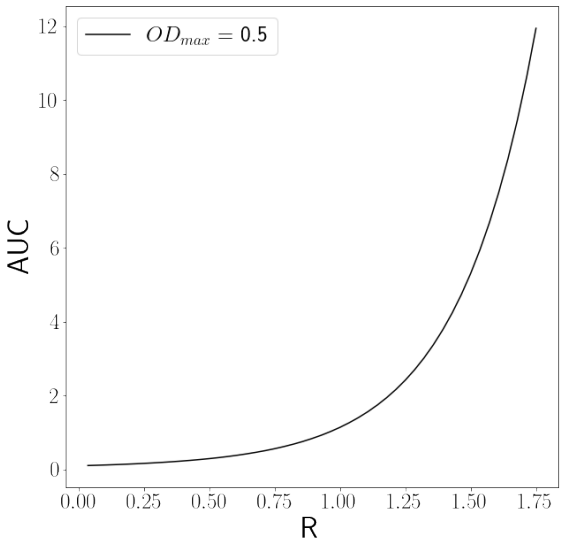

Figure 29: The monotonic behavior of AUC as a function of the growth rate R.

To test the theoretical assumption of interchangeability in the context of the current data, the correspondence between the two rank orders obtained

from the two fitness measures can be quantified through the rank correlation coefficient [24]:

$$\Gamma = \frac{\sum_{i,j=1}^{n} a_{ij} b_{ij}}{\sqrt{\sum_{i,j=1}^{n} a_{ij} \sum_{i,j=1}^{n} b_{ij}}}, \tag{69}$$

where a_{ij} and b_{ij} are the difference between the rank of the ith and the jth genotype in the first order and second order respectively. Γ in the context of the fitness extracted from the current data considering growth rate and the AUC have a value of 0.622 averaged over all concenetrations (with 1 corresponding to perfect correlation). Measuring the same rank order for concentrations below $1\mu/mL$ for which most strains are viable, the rank correlation coefficient falls to 0.263 (Fig. 30). These results indicate weak correspondence between the two measures of fitness which contradicts theory.

Investigating how the resolution of data affects the correspondence between the two measures of fitness, the AUC as a function of the slope is found by

$$AUC = \Delta t^2 [\frac{n}{2} \bar{s} + \sum_{j=1}^{n-1} \sum_{i=1}^{j} s_i] \tag{70}$$

where s_i is the slope of the ith segment (Fig. 31). Taking only few segments into account, the AUC is sensitive to the slope of the first segment, which is in most cases not the provider of the maximum slope (the growth rate). This might explain the poor correlation between the logarithm of the maximum slop and the AUC for the current case.

The weak resolution of the data with only few segments making up the growth curve renders the data a poor representation of the logistic function as already seen in Figure 8. For the same reason, the correspondence of the AUC and the growth rate fails. In the current case, the AUC seems the best option in hand as a measure of fitness because it considers more data points and hence is less sensitive than the growth rate to single point errors.

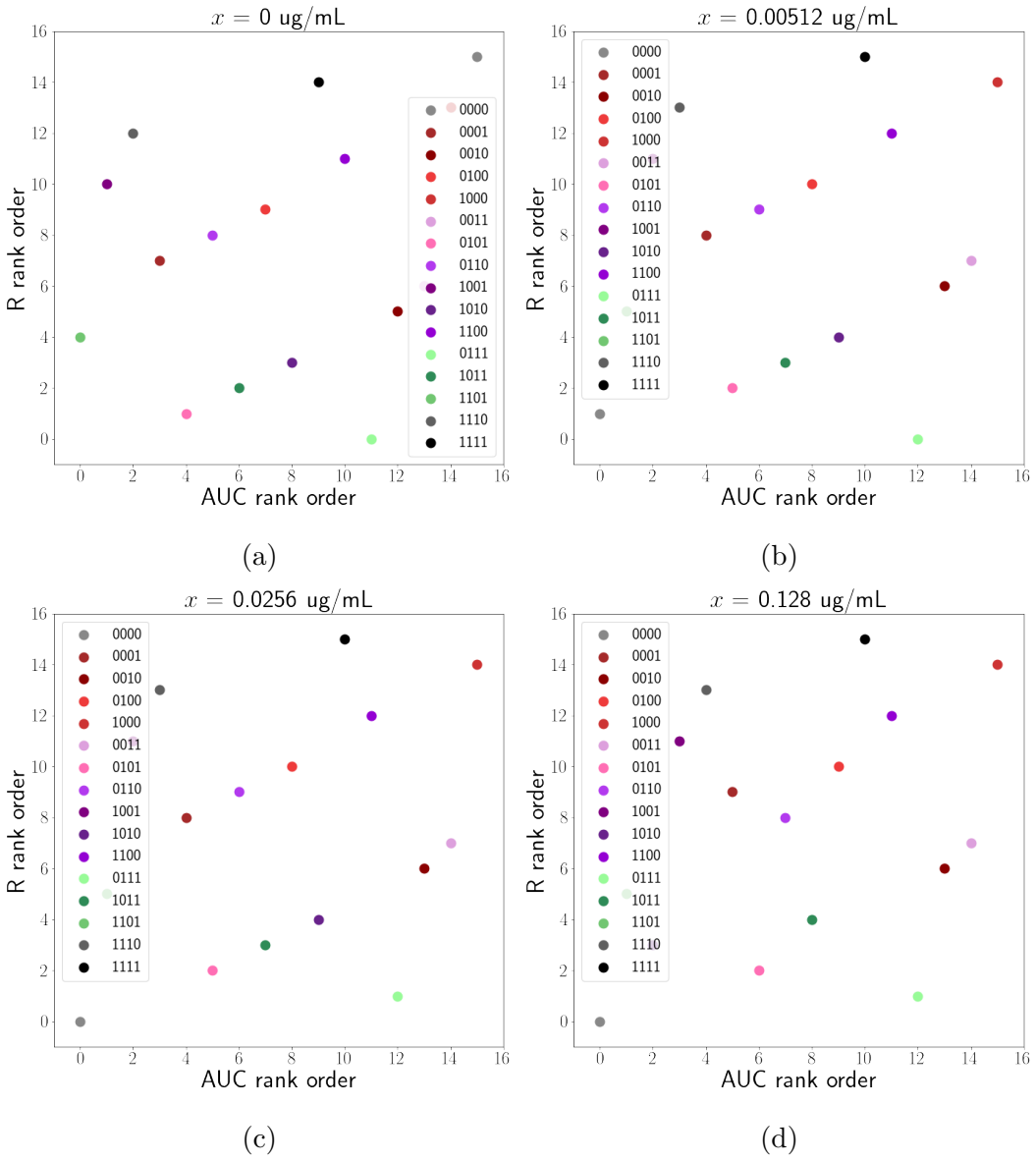

Figure 30: Rank order correlation between AUC rank order and growth rate rank order for the current data. The correlation is weak, where two clusters of genotypes seem to be correlated separately. These two groups of genotypes don't have a trend of common mutations, however it is more likely that the shape of the OD curve and which of the three segments provide the maximum slope are factors in determining the nature of the AUC vs growth rate correlation trend.

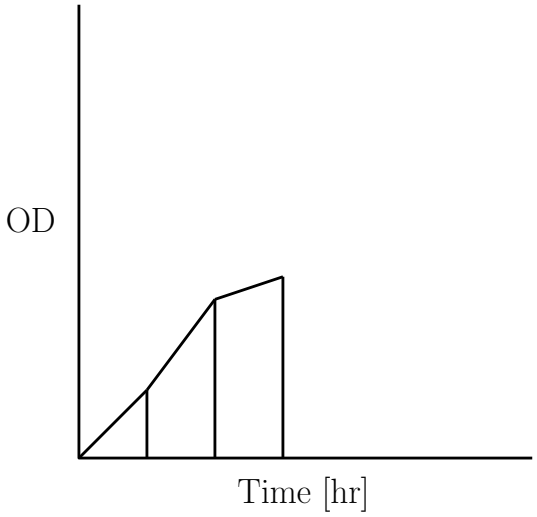

Figure 31: The area under the steady curve (AUC) explained. The part of the data considered create three segements of the shape of a trapezoids.

Experiment results

Mutation	u	v
$\{1\}$	0.13 ± 0.011	4.1 ± 0.067
$\{2\}$	0.18 ± 0.000035	5.2 ± 0.050
$\{3\}$	0.25 ± 0.0066	5.5 ± 0.076
$\{4\}$	0.34 ± 0.021	7.7 ± 0.044

Table 1: Fitted values of u and v for $\alpha = 4$

μ	ν
0.397 ± 0.221	0.709 ± 0.083

Table 2: Fitted values of μ and ν for $\alpha = 4$

The AUC of the full growth curve as the measure of fitness

The analysis of evolution considering the area under the whole curve, including the fluctuating phase, is presented here. The rank orders of the genotypes are different from that considering only the area under the steady part of the curve. Moreover, fitness values of genotypes under intermediate pressure are greater than that in the absence of pressure. That's a general feature, however it is more pronounced here due to the fact that in the fluctuating phase some replicates increased their biomass significantly despite the presence of pressure.

The fitted null-fitness values sometime increased above the wild type's level. The epistasis trend is affected here, where the cost of mutations could either be boosted or damped as in Figure 33 compared to a dominant trend of negative epistasis in cost when the steady phase is only considered. The full AUC landscape is shown in Figure 34, where three genotypes dominate the evolution dynamics throughout the concentration protocol compared to a relatively gradual growth in the number of mutations of peaks when only the steady part of the curve is considered.

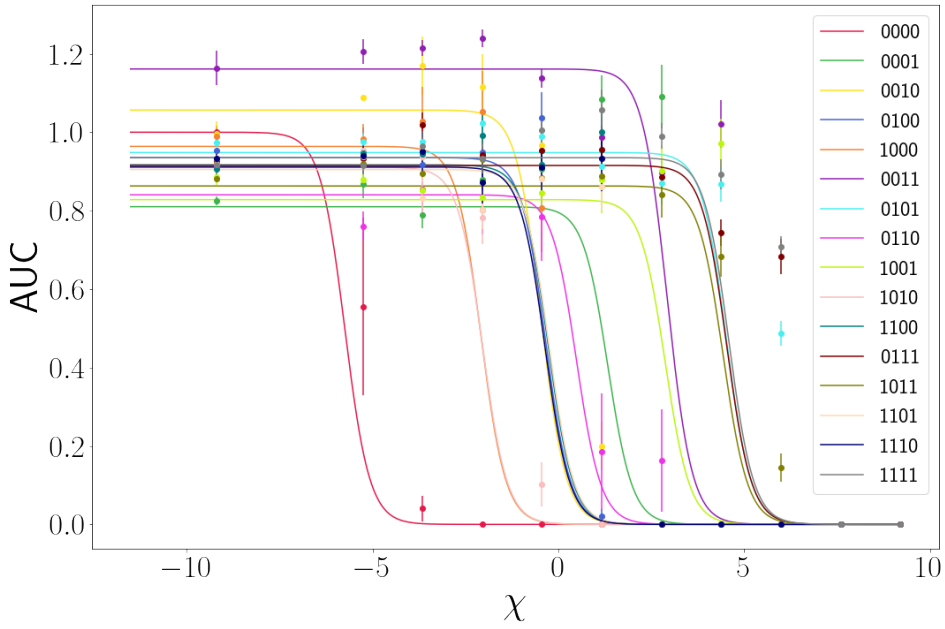

Figure 32: The fitted dose-response curves with the AUC of the full growth curve as a measure of fitness. AUC is normalized with respect to the null-fitness of the wild type and χ is in units of $\log(\mu$ g/ml).

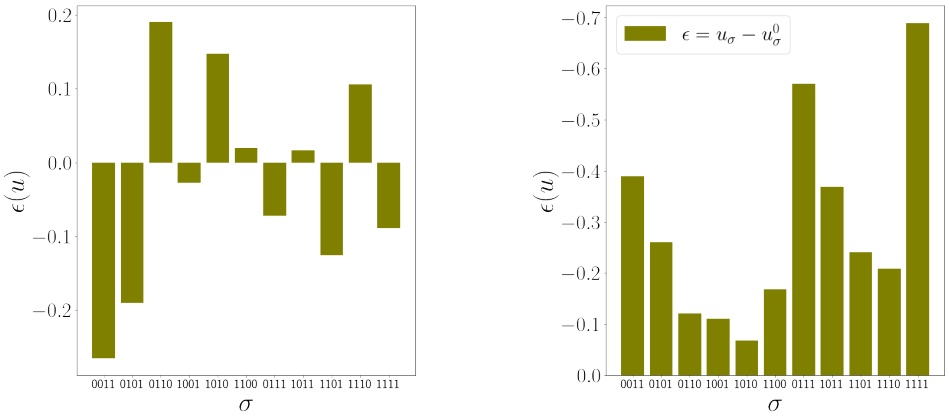

(a) (b)

Figure 33: The epistasis in the null-fitness trend across genotypes considering AUC of the full growth curve (a) vs that of the steady part in (b).

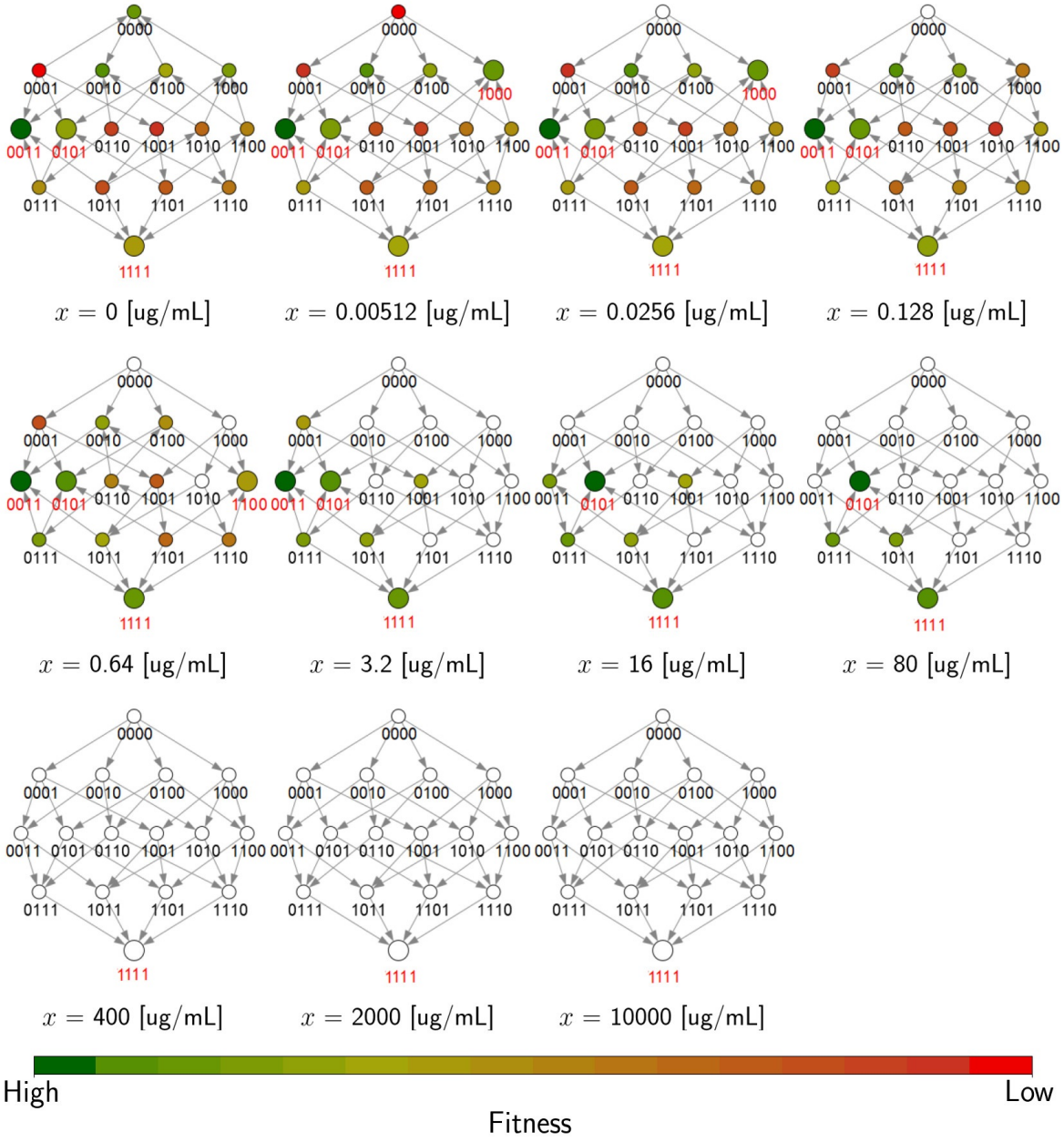

Figure 34: Full landscapes in a changing environment of genotypes considering the entire growth curve including the fluctuating part. Notice how three genotypes dominate the evolution drift throughout the experiment.

Erklärung

Hiermit versichere ich an Eides statt, dass ich die vorliegende Arbeit selbstständig und ohne die Benutzung anderer als der angegebenen Hilfsmittel angefertigt habe. Alle Stellen, die wörtlich oder sinngemäß aus veröffentlichten und nicht veröffentlichten Schriften entnommen wurden, sind als solche kentlich gemacht. Die Arbeit ist in gleicher oder ähnlicher Form oder auszugsweise im Rahmen einer anderen Prüfung noch nicht vorgelegt worden. Ich versichere, dass die eingereichte elektronische Fassung der eingereichten Druckfassung vollständig entspricht.

Köln den 16.10.2024
Muna Turki